TU WIEN

TECHNISCHE
UNIVERSITÄT
WIEN

DIPLOMARBEIT

The magnetic properties of tissue samples and iron-rich organelles from the pigeon Columba livia

Ausgeführt am

Atominstitut, TU Wien

unter der Anleitung von

Privatdoz.Dipl.-Ing.Dr.techn. Michael Eisterer

durch

Daniel Kagerbauer

Baumgasse 44/1/32

1030 Wien

Wien, September 21, 2016

Acknowledgement

I would first like to thank my supervisor Michael Eisterer for always taking time to discuss results and giving advice for further steps. He encouraged me to follow my own ideas but steered me in the right direction, which motivated and challenged me.

Furthermore, I would like to thank David Keays. The door to his office was always open whenever I ran into trouble with my experiments. He had also a lot of patience while describing the necessary parts of Biology to me, thank you for that.

I would also like to thank my colleagues in the low temperature physics group at the Atominstitut and in the Keays lab at the IMP. Thank you for the great time during my thesis, for all the technical conversations and a lot input for my work. It was a great working environment and I had a lot of fun with all of you!

Also, I like to thank my friends for their understanding and their help to clear my mind during the challenging times of my studies.

Finally, I would like to thank my parents for their financial and moral support during my thesis and throughout my studies. They were always there to ask for advice and helping me out.

Abstract

The magnetic sense of animals remains an unsolved puzzle. Over the last few decades a number of different hypotheses have emerged that attempt to explain this phenomenon. One idea, known as the magnetite theory of magnetoreception, predicts that animals such as pigeons employ iron-oxide crystals to transduce magnetic information into a neuronal impulse. To date the identification of such crystals has been challenging because of their small size in comparison to the comparatively large volume of tissue in which they reside. Furthermore contamination of magnetic materials from extraneous sources represents a further obstacle to overcome. In this study I investigate the magnetic properties of ferritin and a variety of pigeon tissues (heart, spleen, liver, hippocampus, upper beak, olfactory bulbs, respiratory concha), using Superconducting Quantum Interference Device (SQUID) magnetometry. In addition I have modelled the magneto-electric properties of an iron-rich organelle, the cuticulosome, implicated in the magnetic sense.

Zusammenfassung

Der Magnetsinn von Tieren ist bis heute ein ungelöstes Rätsel. In den letzten Jahrzehnten sind verschiedene Theorien entstanden um dieses Phänomen zu beschreiben. Eine davon ist die Magnetit Theorie, die vorhersagt, dass sich in bestimmten Zellen von Tiere, Eisenoxid Kristalle befinden, mit denen sie das Erdmagnetfeld detektieren und in einen neuronalen Impuls umwandeln können. Ein großes Problem bei der Identifikation solcher Kristalle ist deren Kleinheit im Vergleich zum umgebenden Gewebe. Außerdem kann es sehr leicht passieren, dass die Probe mit magnetischen Partikeln verunreinigt ist, was eine genaue Bestimmung der magnetischen Eigenschaften erschwert. In dieser Arbeit habe ich die magnetischen Eigenschaften von Ferritin und verschiedenen Gewebearten der Taube (Herz, Milz, Leber, Hippocampus, Schnabel, olfaktorische Bulbus, respiratorische Concha) mit einem SQUID Magnetometer bestimmt. Zusätzlich wurden noch die magnetischen Eigenschaften einer eisenreichen Organelle, dem sogenannten Cuticulosome, im Bezug auf den Magnetsinn untersucht.

Contents

1 Introduction

1.1 Magnetoreception

Magnetoreception is the ability of animals to detect the earth's magnetic field. Especially for animals migrating longer distances such as migratory birds, turtles and fish it is an important input for their navigation system [7][8]. It is known from behaviour studies that these animals use the earth's magnetic field for there long distance navigation, but it is not clear how this sense works on a cellular or even molecular level. There are three different theories for the mechanism behind the sensing of the magnetic field. These are: (1) the radical pair mechanism; (2) the iron based compass theory; (3) the electromagnetic induction theory [9][10][11]. This thesis will focus on the iron based compass theory, but the other theories will be discussed shortly in the next subsections.

It is also not clear which information from the magnetic field animals use to navigate. One idea is that the animals remember a magnetic field map where the magnitude of the earth's magnetic field correspond to a position on the earth's surface. For this the animal needs to memorize the magnitude of the earth's magnetic field in a certain area. It would not be possible for the animal to navigate in an unfamiliar area with this kind of magnetic sense. The other idea is that the direction of the magnetic field is used, especially the angle between horizon and magnetic field vector. Such a sense would work like a compass and allow the animal to navigate in an unknown area. The magnetic sense could also be a combination of a magnetic map and a compass. Then the compass could be used for long distance navigation and the magnetic map for short distance navigation in a known area.

1.1.1 Radical pair mechanism

The radical pair mechanism is a chemical compass where a radical pair is formed in a protein either by breaking a chemical bound or by electron transfer in the protein [9]. The chemical bond has to be broken in such a way that each electron ends up in one radical of the pair. Consequently the two electrons in the radical pair are correlated and form a singlet $|S\rangle$ or a triplet state $|T_+\rangle$, $|T_0\rangle$, $|T_-\rangle$.

$$|S\rangle = \frac{1}{\sqrt{2}} \left(|\uparrow\downarrow\rangle - |\downarrow\uparrow\rangle \right) \tag{1.1}$$

$$|T_+\rangle = |\uparrow\uparrow\rangle \tag{1.2}$$

$$|T_0\rangle = \frac{1}{\sqrt{2}} \left(|\uparrow\downarrow\rangle + |\downarrow\uparrow\rangle \right) \tag{1.3}$$

$$|T_-\rangle = |\downarrow\downarrow\rangle \tag{1.4}$$

It is possible for the singlet state to revert to the starting product or form an end product. For the triplet state it is just possible to form an end product. The biological detection of starting and end
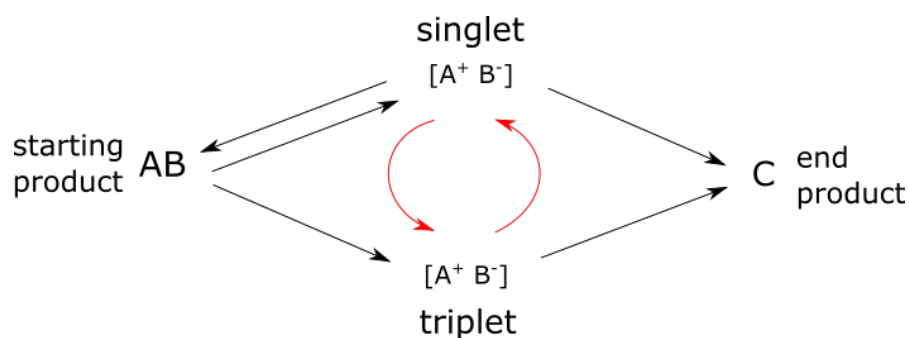
Fig. 1.1: The starting product AB absorbs a photon and becomes a radical pair in ether a singlet or a triplet state, however, just the singlet state can revert to the starting product. The two states can convert into each other due to the nuclear interaction. Furthermore they form an end product C. The relation between AB and C is the signal of such a magnetoreceptor.

products give a relation between singlet and triplet states. The hyperfine interaction between the correlated electrons in the radical pair and the nuclei in the protein drive the conversion between the singlet and the triplet state. This conversion is important because a chemical compass with steady states could not function. A schematic illustration of that is shown in fig. 1.1.

If a magnetic field is applied, the Zemann splitting shifts the energy levels of the states which adds an additional conversion due to the external magnetic field to the faster conversion between singlet and triplet state due to the nuclear interaction. The output of this magnetic field sensor is the ratio between starting and end product which can be further processed to the magnitude of the magnetic field at the position of the sensor.

A candidate protein are the cryptochrome proteins located in the retina. Cryptochromes are blue-light sensitive, and have the capacity to form a radical pair when a photon is absorbed. The idea is that the cryptocromes are placed on the half sphere surface of the retina which enables them to provide directional information about the magnetic field vector. The magnitudes on a two dimensional surface are not enough to calculate the direction of a field vector in three dimensions, additional information like the position of the horizon is required. If the horizon is visible that could be provided by the visual system and in squalid weather conditions the information could come from the sense of balance.

All that together would enable the detection of the direction and the magnitude of the magnetic field vector, however it is really important that the correlation time of the two electrons in the radical pair is in the order of microseconds. That is the timescale where the biological system can detect the start and end products of the reaction. For timescales bigger than the correlation time it is not valid to describe the two electrons as one state, and therefore it would not be possible to detect the earth's magnetic field with such a chemical compass.

1.1.2 Iron based compass

The iron based compass is hypothesised to involve a particle in the cell which can interact with the earth's magnetic field. If such a particle has a remanent magnetic moment there are two different ways how it could interact with a magnetic field. The first is a force on the particle which is described by (eq. 1.5) where $\vec{m}$ is the magnetic moment and $\vec{B}$ the magnetic field.

$$\vec{F} = \vec{\nabla}\left(\vec{m} \cdot \vec{B}\right) \tag{1.5}$$

This force requires a gradient of the magnetic field. The earth's magnetic field is homogeneous on small scales and therefore the gradient is negligible. This interaction would result in an even smaller force which could not be detected by a cell.

The second way a particle could function as a magnetoreceptor is based on torque. A torque on a magnetic moment in a magnetic field is described by (eq. 1.6).

$$\vec{T} = \vec{m} \times \vec{B} \tag{1.6}$$

If the magnetic moment points in the same direction as the magnetic field the torque is zero. The maximum torque is achieved if the magnetic moment is perpendicular to the magnetic field.

The particles in the cell are so small that they are single domain particles. A single domain particle is a particle where just one magnetic domain fits in. In a perfectly spherical particle the magnetic moment can rotate more or less freely without moving the particle itself. Therefore the external magnetic field just rotates the magnetic moment and not the particle. So there is no force which can be detected by the cell.

If the particle is not perfectly spherical it has an easy magnetic axis. That is the direction in which it is easier to magnetize it. This effect depends on the geometry of the particle. Such a particle could be aligned in an external magnetic field and transfer a force that could be detected by a cell. This alignment is used by magnetotactic bacteria. There are many types of these bacteria, a TEM image of one kind is shown in fig. 1.2. In their cells there are magnetite particles with a diameter of 30 nm in a several nm long structure shaped like a compass needle [12]. This anisotropy permits the magnetic moment pointing along the axis of the bacteria. In the earth's magnetic field a torque on the whole bacteria aligns it with the magnetic field lines. This enables the bacteria to move along such magnetic field lines [12].

If there is no particle with a remanent magnetic moment in the cell it is also possible that a particle is magnetized in the earth's magnetic field. The direction of the magnetization depends on the easy magnetic axis of the particle. If the easy axis points in another direction then the earth's magnetic field there could be a torque on a particle because the magnetic moment tries to align with the external magnetic field.
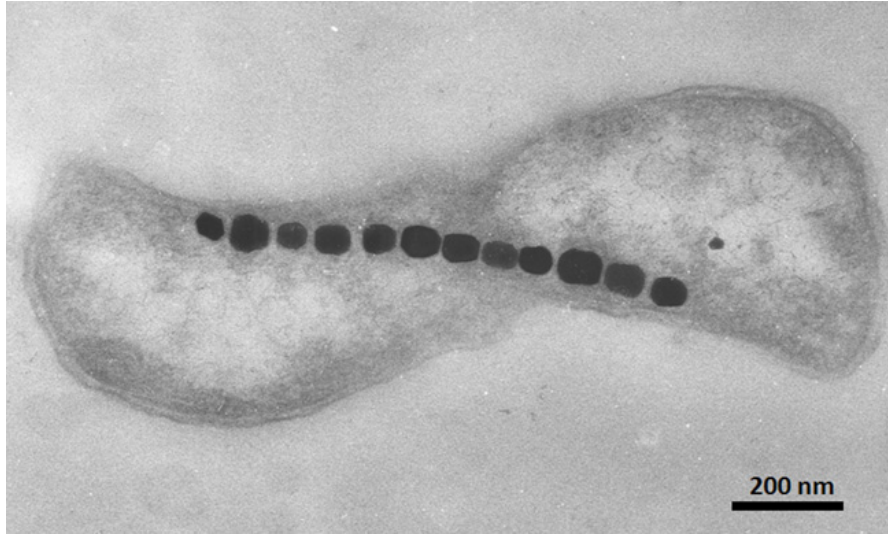
Fig. 1.2: TEM image of a magnetotactic bacteria with a chain of magnetite particles to align in the earth's magnetic field [19].

1.1.3   Electromagnetic induction

Another way to get a detectable signal is electromagnetic induction where a varying magnetic field induces a voltage in a conducting loop. A voltage signal is ideal because it could be processed directly by the biological system. The induced voltage is defined as follows:

$$u = -\frac{\partial}{\partial t} \int \vec{B} \, d\vec{A} \tag{1.7}$$

There the magnetic field $\vec{B}$ is integrated over the enclosed area A. The vector $d\vec{A}$ is the normal vector of the infinitesimal area element dA. The varying magnetic field could be produced by a moving magnetic moment. Close to the particle the dipole field is larger which would result in a higher induced voltage. So it would be most efficient to place the conducting loop close to the particle with the magnetic moment.

Another way to use induction to detect the earth's magnetic field is a loop in the animal's head. If the head is moved the flux through the loop changes and there is a voltage induced. This system also works for the more or less constant earth's magnetic field. The voltage in the loop could then be detected with an electroreceptor [11].

It is very important for all iron based compass theories to identify the particles which interact with the earth's magnetic field. That could be done by characterising the magnetic properties of various tissues. If there are no tissues with remanent magnetic moments the induction mechanism is most likely to produce the signal that is detected by the biological system.

1.2   Types of magnetism

This section will give an overview of the types of magnetism important for magnetoreception. These are especially the types of magnetism where the exchange interaction between the spins is stronger then the thermal energy. For all these types there is a critical temperature under which the exchange interaction becomes stronger then the thermal energy. Above this temperature the materials behave like paramagnetic materials, because the single spins undergo thermal movement and are no longer ordered. Another type of magnetism discussed in this section is superparamagnetism which is important for small particles where just one magnetic domain fits in.

1.2.1   Ferromagnetism

In a ferromagnet below the critical temperature, called the Curie temperature, the internal spins align parallel which minimizes the energy of the system. Due to the short range of the exchange interaction the alignment is not present on a macroscopic scales. At longer ranges the dipole-dipole interaction between the spins becomes stronger and the spins tend to align antiparallel. This results in the formation of magnetic domains, so called Weiss domains, in which the spins are aligned parallel, but the spins in different domains are aligned randomly with respect to each other. The size of such a magnetic domain can range up to 10 μm [13].
Single domain ferromagnetic particles would be good candidates for an iron base compass because all spins are aligned which result in a big magnetic moment. The maximum size is around 100 nm which would fit in a cell of 10 μm. It would also be important to make the particles biologically compatible. This could be a problem because most ferromagnets are composed of F, Ni or Co and their respective alloys.

1.2.2   Anitferromagnetism

In antiferromagnets the spins are align antiparallel below the critical temperature, called Neél temperature. The antiferromagnet can be imagined as two intertwined ferromagnets with a lattice parameter twice as big as the one of the antiferromagnet. Furthermore all the spins have the same magnitude. This results in an overall vanishing magnetic moment, because the single spins compensate each other. Single domain antiferromagnetic particles can carry a non vanishing magnetic moment due to uncompensated spins on the surface. Thus the magnetic moment of a single domain antiferromagnetic particle is smaller than a single domain ferromagnetic particle with the same size.

1.2.3   Ferrimagnetism

In ferrimagnets the exchange interaction also favours antiparallel alignment of the spins. In contrast to a antiferromagnet the spins of the two sub lattices have different magnitudes which results in a non vanishing magnetic moment of a ferrimagnet. The magnetic moment is still

smaller than the magnetic moment of a ferromagnet of the same size, because there is a partially compensation of the spins.

1.2.4   Superparamagnetism

The particles required for an iron based compass need to have a certain size to fit into a cell with a diameter of 10 μm. This limits the size of a iron based compass, because not all of the cell can be occupied by such a particle. A size of 1 to 100 nm would fit into the cell which is in the order of the size of one magnetic domain. Therefore the interesting particles for an iron based compass are single domain particles. An example of such a particle is ferritin which is described in more detail in sec. 1.3.

Each single domain particle has a magnetic moment pointing in an arbitrary direction. If one applies a magnetic field the energy of the particle is the potential energy of the magnetic moment in the external field.

$$E_{pot} = -\vec{m} \cdot \vec{B} \tag{1.8}$$

This energy (eq. 1.8) depends on the angle between magnetic moment $\vec{m}$ and applied magnetic field $\vec{B}$. If there are more than one particle at a certain temperature their angles are randomly distributed. With an applied magnetic field there will be an Boltzmann distribution of the angles. The magnetization of the particles can be calculated by thermodynamical averaging the angle over the Boltzmann distribution. This yields the Langevin function as for a normal paramagnet. Therefore the treatment of a superparamagnet is in principle the same as for a normal paramagnet. The difference is that the magnetic moments are not from the atoms but result from the single domain of a ferromagnet. This usually results in a bigger saturation magnetization of a superparamagnet than of a normal paramagnet.

Until now the description is just valid for isotropic particles. If the particle has an uniaxial anisotropy there is an extra term added to the energy. This results in a different Boltzmann distribution for the angels. The distribution also changes if not all particles have the same volume.

The magnetic moment of a single domain particle undergoes a Brownian motion like fluctuation in an applied magnetic field [1]. If the magnetic field is changed, this fluctuation cause the magnetization of the particles to decay towards its equilibrium.

$$\tau = \tau_0 \, exp \left(\frac{KV}{k_B T} \right) \tag{1.9}$$

The relaxation time τ depends on the volumes of the single particles V and the temperature of the system [2]. τ_0 is a characteristic time scale and depends on the material. K is the anisotropy energy of a particle per unit volume. A superparamagnet can now either have a short relaxation time which would cause the magnetization to decay or a long relaxation time which would result in a remanent magnetic moment.

It is important to take the relaxation time into account for temperature dependent measurements of the magnetic moment of a superparamagnet. It takes a certain time to measure the magnetic moment of a sample. If the measurement time is larger than the relaxation time, the magnetic moment has another value than for the opposite case. That appears in a difference between a field cooled and a zero field cooled measurement. For the zero field cooled measurement the sample is cooled down without field. Then a magnetic field is applied and the measurement starts from low to high temperatures. The magnetic moment increases at the beginning with increasing temperature. It forms a maximum at a certain temperature and starts to decrease with increasing temperatures. That is explained with the difference between measurement and relaxation time. At low temperatures the relaxation time is longer than the measurement time and the magnetic moment can not decay during the measurement. The relaxation time deceases with increasing temperature. At the so called blocking temperature T_B the relaxation time becomes shorter than the measurement time. The temperature is called blocking temperature because at temperatures below the blocking temperature the relaxation times is so large that the magnetic moment is blocked.

For the field cooled measurement a magnetic field is applied and the magnetic moment is measured from high to low temperatures. The magnetic moment increases with decreasing temperature for the whole temperature range. There is no peak in the magnetic moment at the blocking temperature because the single magnetic moments of the whole superparamagnet are aligned from beginning on with the applied magnetic field.

1.3   Ferritin

Ferritin is the main iron storage protein in biological systems [14]. It is necessary to store the iron in a protein because free iron is toxic for biological systems. The protein consists of an outer shell and an inner core where the iron is stored. The diameter of the protein shell is around 12 nm and independent of the amount of iron stored in the protein. There could be up to 4500 iron atoms stored in one ferritin protein. If the protein is fully loaded with iron the diameter of the core is about 8 nm.

For the magnetic properties only the iron containing inner core of the protein is important. The magnetic moment of the protein shell is a small diamagnetic background. Inside the iron core the iron atoms are ordered antiferromagneticaly [3][14]. The Néel Temperature of this antiferromagnetic state lays above room temperature which is shown in [3] and replicated in sec. 3.1. Therefore one ferritin protein has a remanent magnetic moment at room temperature arising from uncompensated spins of iron atoms at the surface of the iron core. Ferritin contains just one magnetic domain which makes it a single domain magnetic nanoparticle that behaves collectively, for example in a liquid, like a superparamagnet.

Magnetization curves of ferritin can be divided in two sectors. Below the blocking temperature the magnetization curve shows a hysteresis which is a relaxation time phenomena. Above the blocking temperature ferritin should behave like a paramagnet with higher saturation magnetiza-
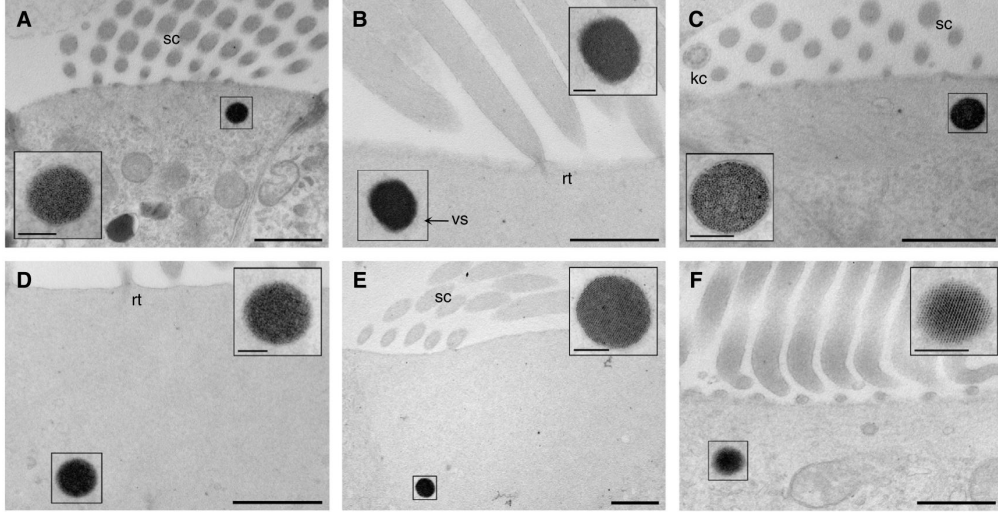
Fig. 1.3: TEM images of hair cells with iron rich organelles, the cuticulosomes. They are located in the lagena (A and D), basilar papilla (B and E), utricle (C), and saccule. The cuticulosome is composed of smaller particles with a diameter of around 8 nm. The scale bares represent 1 μm [6].

tion. Therefore the field dependence of the magnetic moment should be described by a Langevin function, however, there is an additional term that needs to be considered:

$$m(H,T) = m_0\, L\left(\frac{m_i B}{k_B T}\right) + \chi\, H \tag{1.10}$$

$L(x) = \coth x - \frac{1}{x}$ is the Langevin function. m_i is the magnetic moment of one single ferritin protein. The additional term $\chi\, H$ could be understood as the bulk susceptibility of the antiferromagnetic grains.

1.4   The cuticulosome

It has been reported that after exposure to a rotating magnetic field pigeons show brain activity in a region that is associated with the vestibular system [15]. This lead to the discovery of an iron rich organelle in the curticular plate of pigeon hair cells [6]. They are located in the cochlea and vestibular sensory epithelium of the pigeons. The TEM images in fig. 1.3 show that these organelles, called cuticulosomes, are composed of electron dense nano particles. The cuticulosome has a diameter of around 500 nm and the nano particles have a diameter of around 8 nm [6]. Recent studies have shown that the particles in the cuticulosome are mainly ferritin and the diameter of the electron dense particles are also in agreement with the diameter of the iron core of ferritin (see 1.3).

The location of the cuticulosome would be ideal for a magnetoreceptor because it is located in a hair cell which is a sensory receptor. This could provide the signal processing into the nervous

system. In sec. 3.3 it will be discussed how the cuticulosome could function as a magnetoreceptor.

1.5   Motivation

The aim of this thesis is to expand our understanding of the physical basis of the magnetic sense in pigeons. Specifically the goals of this thesis are:

1. Design a sampleholder for the SQUID magnetometer to measure small magnetic moments.

2. Measure the magnetic properties of a broad range of pigeon tissues using a SQUID magnetometer.

3. Model the magnetic properties of the cuticulosome.

2 Materials and methods

2.1 SQUID magnetometer

The magnitudes of the magnetic moments of biological tissue are in a wide range. In tissues containing more blood the magnetic moments are bigger, however in other tissues the magnetic moments are very small. Therefore, it was necessary to use a magnetometer with a wide sensitivity range, for which a SQUID magnetometer is ideal. It is the most sensitive magnetometer but it is still possible to measure higher signals. Furthermore one can apply fields up to 7 T in our Quantum Design MPMS XL SQUID magnetometer and also measure temperature dependence from 5 K up to room temperature.

We performed two kinds of measurements in the SQUID magnetometer. The first was the measurement of the magnetic moment of the sample as a function of the applied magnetic field, which could show us a possible hysteretic behaviour of the sample. These measurements were performed at 5 K because that minimizes the thermal noise and makes it easier to measure small signals. The other performed measurement was the magnetic moment as a function of the temperature with a constant applied magnetic field. With this measurement it was possible to access the difference of zero field cooled and field cooled measurement of superparamagnetic material.

2.1.1 Functional principles

In a SQUID magnetometer the magnetic moment of a sample is measured by a SQUID sensor. The signal is transferred with a flux transformer from the sample space to the SQUID sensor. This is necessary because the SQUID should be in liquid helium and in the sample space it is possible to set different temperatures with the helium flow. Furthermore it is important to keep the SQUID sensor away from any magnetic noise like the magnet that applies a magnetic field to the sample. A second order gradiometer is build in the flux transformer (shown in fig. 2.1) which
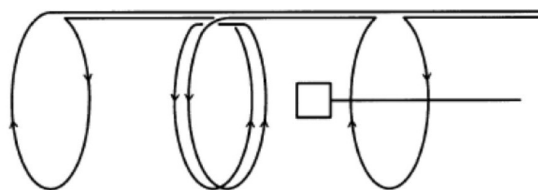
Fig. 2.1: Gradiometer of the SQUID magnetometer with a sample in it [4]

subtracts a constant and a gradient magnetic signal. For the measurement the sample is pulled through this gradiometer and the SQUID sensor gives a specific output signal. The software of the device assumes that the signal origins from a point like dipole and fits such a signal to the output. For bigger samples that assumption is not totally true but gives a reasonable value for the magnetic moment.

All measurement points are an average value of ten measurements. The errorbars in the plots correspond to the standard deviation calculated from these ten measurements. During some measurements there occurred one or several jumps in the measured voltage. The software does not detect this and provides erroneous measurements. They are also used for the averaging which results in a value way of the actual magnetic moment and a big standard deviation. Such points do not show any behaviour of the sample, but are only from the data evaluation. These measurement points where not removed from the data, however the raw data files were recorded and one could clearly see such voltage jumps there.

After applying a magnetic field to the sample it was important to wait for at least one minute, because otherwise the drift in the measured signal is too big and the software is not able to subtract it appropriately. The waiting time depends on the size of the magnetic field change. The bigger the change the longer one should wait. For example, after a magnetic field change of 7 T a waiting time of 1 min is too short, there a waiting time of at least 3 min is advisable.

2.1.2   Sample holder

The sample holder is the part where you mount your sample on and transfer it to the pick up coil system of the SQUID sensor in the cryostat. Therefore, it is very important that the signal of the sample holder is smaller than the signal of the sample itself. One can always subtract the signal of the sample holder from the signal with sample, which could correct the measured signal. However, it is problematic if the signal of the sample and the signal of the sample holder are of the same magnitude. Then a subtraction of these two would magnify small variations in the signals which result in signals that are just noise.

There are further restrictions to the sample holder because of the measurement process in the SQUID (described in sec. 2.1.1). The sample holder has to be long enough that a part of the sample holder is always inside the gradiometer during the measurement. Moreover the sample holder has to be translation symmetrical along the axis where it is pulled through the gradiometer. If these restrictions are not fulfilled it would result in a signal from the the sample holder that could be misinterpreted as a signal from the sample.

When performing SQUID analysis the choice of sample holder is a critical factor. We considered three options for the experiments: (1) straw; (2) quartz glass tube; and (3) aluminium foil. The usual sample holder for SQUID measurements are normal drinking straws [4]. They are easy to handle and fix to the transportation rod of the SQUID. In such a straw the sample is placed in a gelatin capsule. The disadvantage of this kind of sample holder is that the signal is bigger or at least of the same magnitude as the signals we want to detect. The geometry of the gradiometer in the SQUID makes it possible to design a compensated sample holder (see fig. 2.2. There five gelatine capsules are fixed at the sample holder with the same distance between them. This distance is the displacement of the outer coils from the middle coil of the gradiometer. The coils of the gradiometer are wound in opposite direction, which subtracts the signal of the capsules in the outer coils from the signal of the capsule in the middle coil with the sample in it. During the
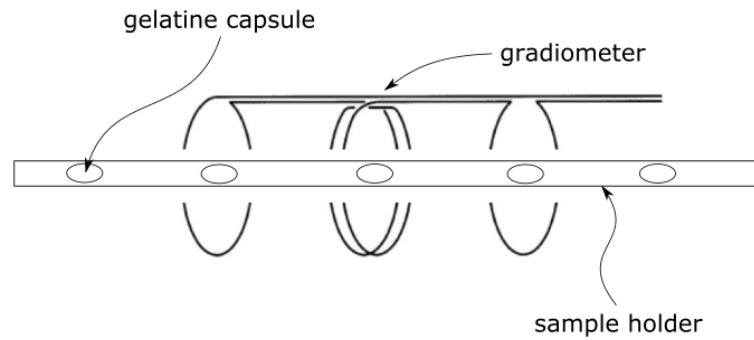
Fig. 2.2: Sample holder with compensation capsules in the gradiometer. The sample is placed in the capsule in the middle and the other capsules compensate the signal it.
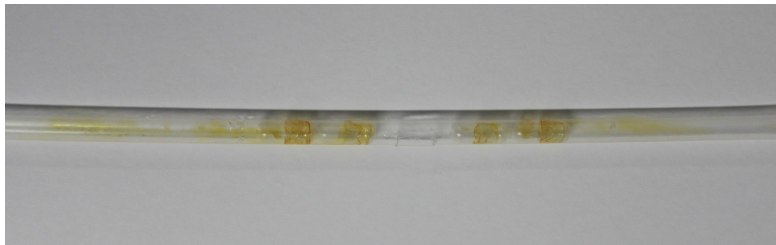
Fig. 2.3: Straw as sample holder with compensation capsules. In the middle a window is cut in the straw to easy change the capsule with the sample in it. The other four capsules are fixed with vanish to the straw.

measurement the sample holder is pulled through the gradiometer. The two further capsules on the sample holder make sure that the signal is subtracted during the whole measurement process. In fig. 2.3 a straw with compensation capsules is shown. Fig. 2.4 shows how compensation works for a field of 1 T, but for higher fields the inhomogeneities in the straw start to contribute to the signal. Therefore the straw or the straw with compensation capsules is not the ideal sample holder for our applications.

To minimize the background signal one has to use a material for the sample holder with a low magnetic moment. Moreover it is preferable that the sample holder is as light as possible because the magnetic moment increases with the mass. One possibility is quartz glass, however they are hard to cut and that makes it difficult to cut slits for the sample in the sample holder. Another good material for a sample holder is aluminium. It is available as foil which makes it easy to fold and it is very homogeneous from its production process. Furthermore one can fold a translation symmetric u-profile to easily change the sample. Such a sample holder is shown in fig. 2.5.

In fig. 2.6 the magnetic moment as a function of the applied field is shown for the different sample holders. The sample holder made of aluminium foil does not have the smallest magnetic moment but because it is easier to handle than the quartz glass tube it is the best choice for
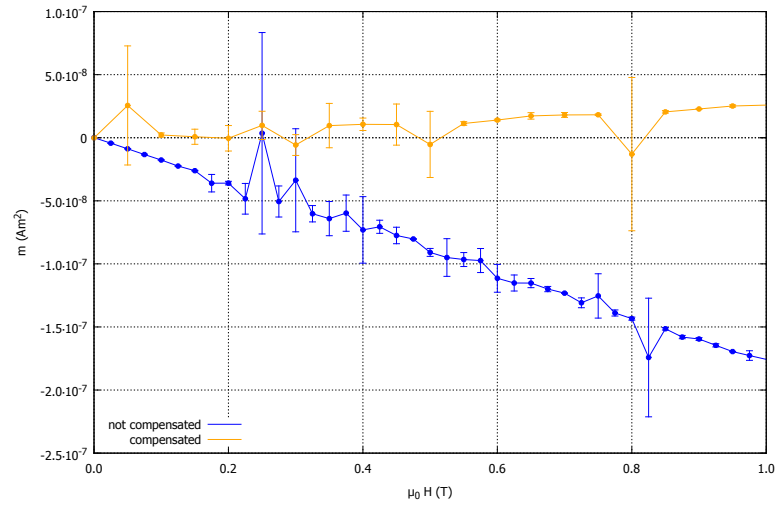
Fig. 2.4: Comparison of the magnetic moment of the straw with one gelatine capsule and the straw with 5 gelatine capsules as compensation. The errorbars show the standard deviation of the averaged ten measurements.
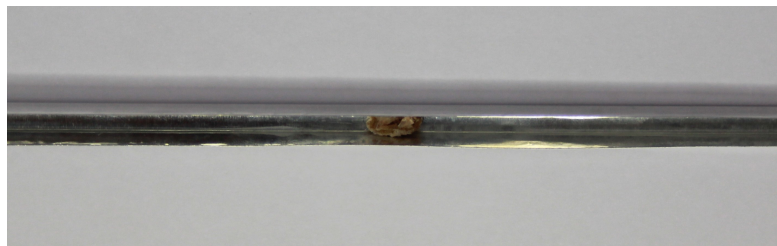
Fig. 2.5: Aluminium sample holder. The sample is placed in the middle of the sample holder with vacuum grease.
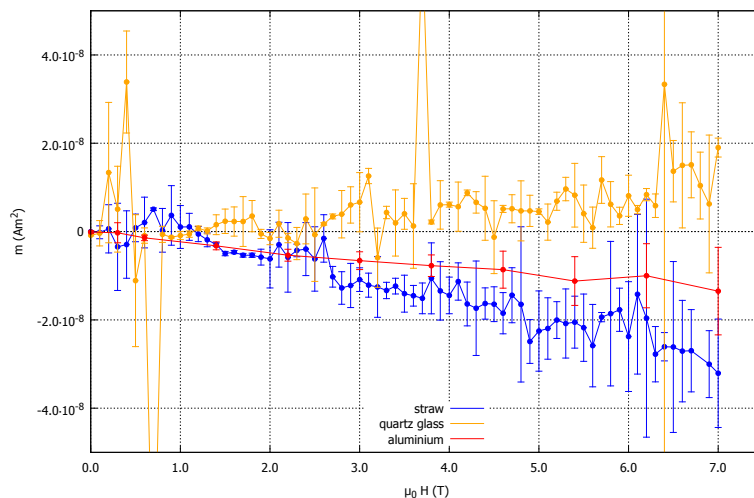
Fig. 2.6: Comparison of the field dependence of the magnetic moment of a straw sampleholder, a sampleholder made of aluminium foil and a quartz glass tube as sampleholder. The errorbars show the standard deviation of the averaged ten measurements.

our requirements. We fixed the sample to the aluminium holder just with a small amount of vacuum grease. To subtract the background signal the sample holder plus vacuum grease were first measured alone in advance of the measurement with the sample. We concluded that an aluminium sample holder would be best suited to measure biological samples.

2.2   TXRF spectroscopy

A Atomica 8030C TXRF spectrometer was used to measure the iron content of the tissue. Total reflection x-ray fluorescence analysis (TXRF) is a x-ray based spectroscopy measurement where a Mo x-ray tube is used to excite the sample. In contrast to the normal XRF spectroscopy the x-ray beam hits the target under the total reflection angle. The set-up is shown in fig. 3.30.

This set-up minimizes the scattering radiation at the position of the detector. Furthermore it is possible to position the detector closer at the sample to detect fluorescence radiation with lower intensity. The sample is exited twice because the x-ray beam hits it under the total reflection angel.

The sample has to be in a liquid form for the measurement to make sure that it is applied as a thin film on the reflector. The samples were dissolved for at least 24 hours in a mixture of one part HNO_3 and three parts HCl called aqua regia. Afterwards a known concentration of Gallium, comparable to the concentration one wants to measure, was added as internal standard. The dissolved sample with the internal standard was evaporated on the reflector to obtain a thin film of the sample. With the known concentration of the internal standard the measurement software is able to calculate the concentration of other elements. Furthermore the excitation energy of
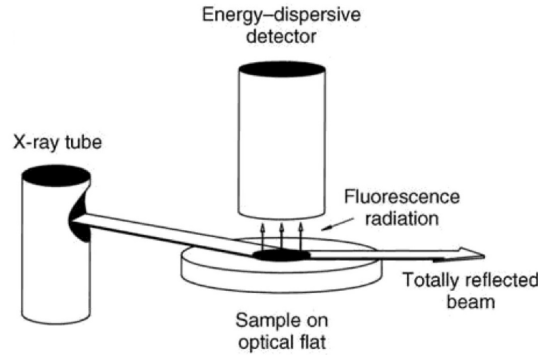
Fig. 2.7: Set-up of a TXRF spectroscope

the internal standard element should not be too far away or too close to the excitation energy of the element one wants to detect. We want to detect iron and therefore gallium is a good internal standard.

2.3   Sample preparation

It was important to avoid contaminations during the sample preparation. We only used titanium, plastic or ceramic tools for the dissection. Moreover all eppendorf tubes for the sample storage were cleaned with 30% HCl and afterwards washed with distilled water. All that should minimize the chance of contamination with magnetic particles from the lab environment. However, it is still important to make sure that signals are from the sample and not from any contamination of the tissue. This contamination could come from the cages of the birds or iron particles from the laboratory environment.

After dissecting the tissues they were frozen in the cleaned tubes in liquid nitrogen. All samples were freeze dried in a commercial freeze dryer Christ Alpha 2-4 LD plus at least for 24 hours to remove the water which would be a background signal in the measurements.

2.4   Possible contaminations

As mentioned in sec. 2.3 it is important to ensure that the samples are not contaminated during the sample preparation. However, further contaminations from the tissue itself are blood and water. If one estimates, that after the freeze drying 1% of the sample is still water that would lead to a magnetic moment of $-6.3 \cdot 10^{-12} \mathrm{Am}^2$. This value is calculated with the magnetic susceptibility of water $-9 \cdot 10^{-6}$ [22] and an average sample mass of 10 mg. The background signal of such an amount of water is smaller than the detection limit of the SQUID magnetometer. The magnetic moment of blood was measured as a function of the temperature at 1 T to estimate the contribution to the signals of the tissue samples. For the measurement cotton wool was soaked with blood, frozen in liquid nitrogen and freeze dried. In fig. 2.8 the normalized magnetic moment at 1 T is shown as a function of the temperature. The normalized magnetic moment of blood is
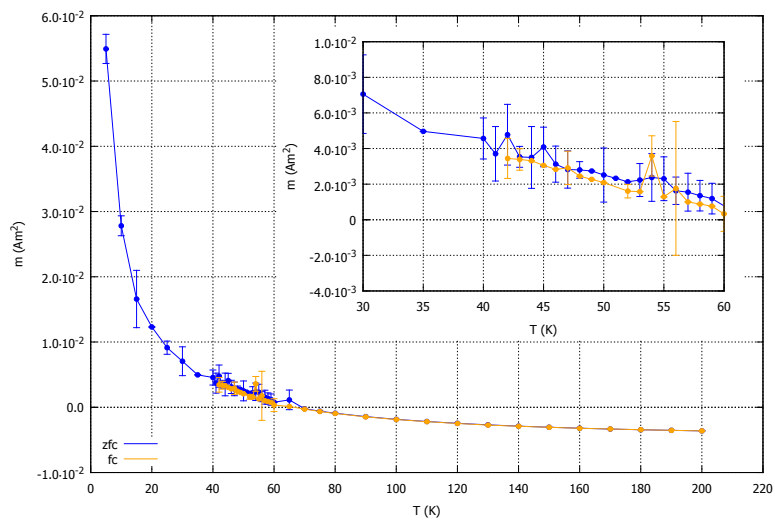
Fig. 2.8: Normalized magnetic moment of cotton wool soaked with 27 mg blood at 1 T. The errorbars show the standard deviation of the averaged ten measurements.

of the same magnitude as the normalized magnetic moment of blood rich tissue samples. This shows that most of the signal of these tissue samples originates from the blood itself.

3 Results

The results section is structured in three subsections. The first one is about the magnetic properties of ferritin which is important, because most of the magnetic moment of different tissues arises from it. The second analyses the magnetic properties of different tissues and in the final section we discuss whether the cuticulosome could act as magnetoreceptor.

3.1 Ferritin

The biggest contribution to the magnetic moment of any tissue comes from iron in the cells and this iron is mainly stored in ferritin [14]. Therefore the magnetic properties of ferritin could help to understand the signals from other tissue samples. We therefore undertook measurements of purified horse spleen ferritin.

In the temperature dependence of the magnetic moment, the blocking temperature is the temperature where the zero field cooled (zfc) and the field cooled (fc) measurement bifurcates (see fig. 3.1).
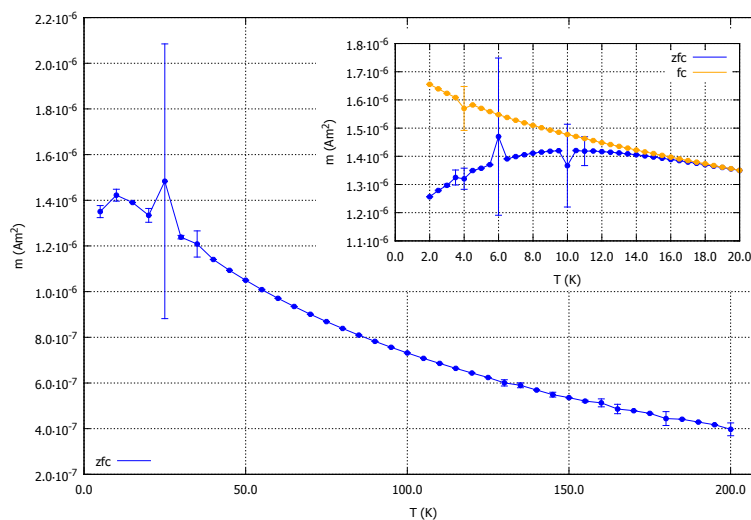
Fig. 3.1: Temperature dependence of the magnetic moment of ferritin. The main plot is a zfc measurement with a coarse temperature resolution between 2 and 200 K. The insert shows the measurement of the same sample with a fine temperature resolution between 2 and 20 K. The insert shows zfc and fc measurements. The errorbars show the standard deviation of the averaged ten measurements.

The blocking temperature is the temperature where the curve of the magnetic moment bifurcates. In our case that is 16 K.

The field dependence of the magnetic moment was measured at 5 K, 10 K and 30 K. This makes it possible to compare the behaviour under, close to and above the blocking temperature. The magnetic loops for 5 K, 10 K and 30 K are shown in fig. 3.2, fig. 3.3 and fig. 3.4, respectively. The
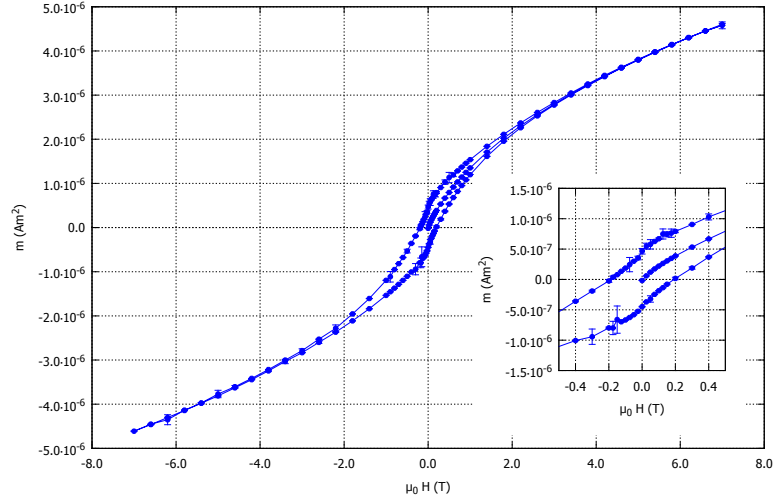
Fig. 3.2: Magnetic field dependence of the magnetic moment at 5 K. The insert shows a zoom of the low field area. The errorbars show the standard deviation of the averaged ten measurements.

biggest hysteresis is at 5 K where the relaxation time of the superparamagnetic particle is bigger then the measurement time and the magnetic moment of the particle is blocked, which results in a remanent magnetic moment of the ferritin. At 10 K the hysteresis is smaller than the one at 5 K but still detectable because 10 K is beneath the blocking temperature of the sample. The measurement at 30 K shows no hysteresis as the temperature is above the blocking temperature. This means that the relaxation of the magnetic moment is faster than the measurement time, which results in a paramagnetic behaviour because the magnetic moment is no longer blocked and can align with the applied magnetic field. Moreover, in all plots the linear term in the magnetic moment (eq. 1.10) is visible. It dominates at higher fields because there the Langevin function is already saturated.

For further investigation these magnetization loops were measured at different temperatures and eq. 1.10 was fitted to the data. The fit parameters were the saturation magnetization, the magnetic moment of a single ferritin protein and the susceptibility of the linear term. The magnetic moment of a single ferritin was limited to a range around the known magnetic moment of approximately 350 μ_B. The data with the fit functions is shown in fig. 3.5. In general the fit is in good agreement with the data, but it is better for higher temperatures. The temperature dependence of the saturation magnetization is shown in fig. 3.6. For the measured temperature range the temperature dependence of the fit parameter is linear. With an extrapolation of the linear fit one can find the temperature where the saturation magnetization vanishes [3]. This extrapolation suggests an ordering temperature of approximately 330 K. The extrapolation could be improved with measurement points at higher temperatures, however at these temperatures ferritin liquefies and could destroy the gelatine capsules. An ordering temperature above room temperature shows indirectly that the single ferritin molecules have a remanent magnetic moment
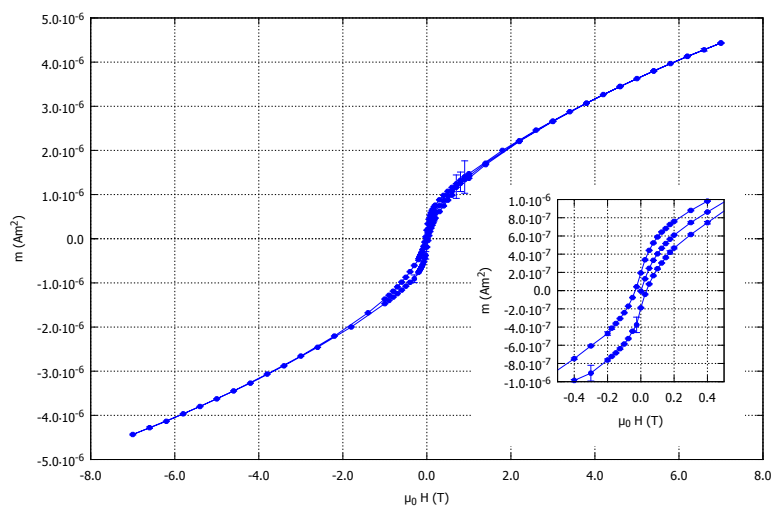
Fig. 3.3: Magnetic field dependence of the magnetic moment at 10 K. The insert shows a zoom of the low field area. The errorbars show the standard deviation of the averaged ten measurements.
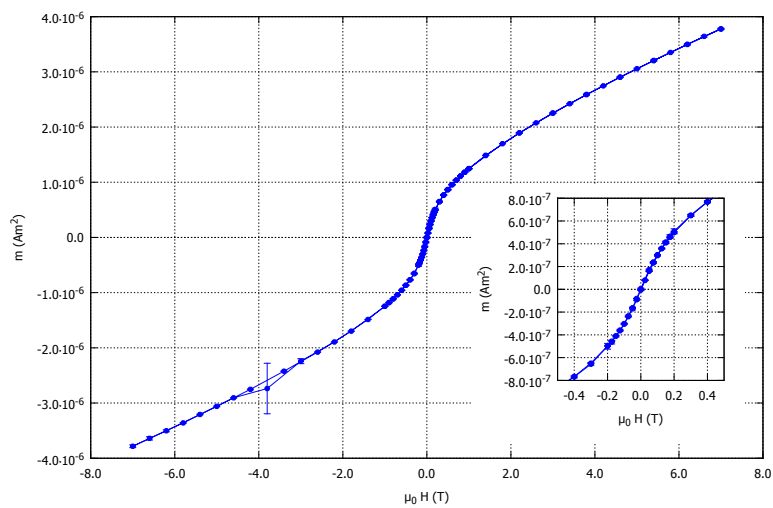
Fig. 3.4: Magnetic field dependence of the magnetic moment at 30 K. The insert shows a zoom of the low field area. The errorbars show the standard deviation of the averaged ten measurements.
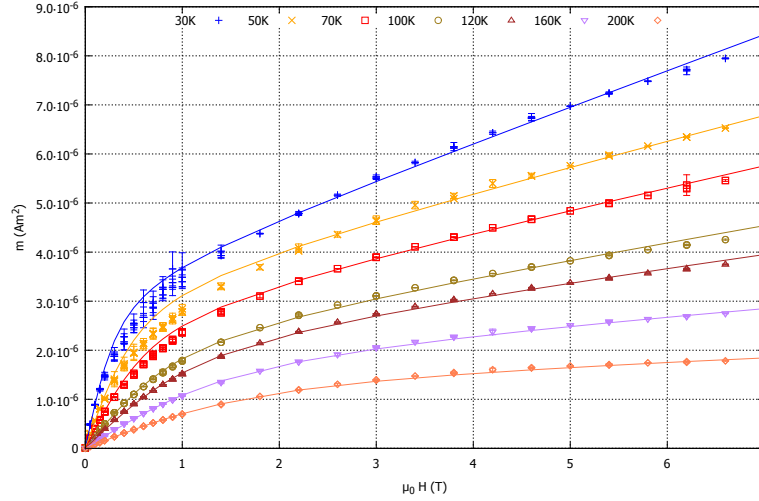
Fig. 3.5: Magnetic field dependence of the magnetic moment of ferritin at various temperatures. The solid lines represents a fit of eq. 1.10 to the magnetization data of the ferritin sample. The errorbars show the standard deviation of the averaged ten measurements.

at room temperature.

Another fit parameter was the susceptibility of the liner term in eq. 1.10. The temperature dependence of this parameter is shown in fig. 3.7. It decreases with increasing temperature which could be ascribed to the faster movement of the particles at higher temperatures and therefore more randomization.

The temperature dependence of the magnetic moment of one single ferritin nano particle is shown in fig. 3.8. There one can see a small increase of the magnetic moment with increasing temperature. The magnetic moment of ferritin arises from uncompensated spins at the surface. An increasing temperature could increase the number of uncompensated spins at the ferritin surface. These uncompensated spins are responsible for the magnetic moment of ferritin, which increases if there are more surface spins. A further increase of the temperature should start to decrease the magnetic moment due to thermal fluctuations in the ferritin core which is shown in [3]. The mean value of the magnetic moment of a single ferritin protein ranges in the expected area. Showing that ferritin has a remanent magnetic moment at room temperature allows us to construct theories of superparamagnetic tissues with ferritin as building block.

3.2   Tissue samples

Next we measured the magnetic moment of a range of pigeon tissues, with the aim of narrowing the search for an iron-based magnetoreceptor. Specifically we analysed the: liver, spleen, heart, olfactory bulbs, hippocampus, respiratory concha, and upper beak.

The magnetic field and temperature dependence of the magnetic moment of the samples were
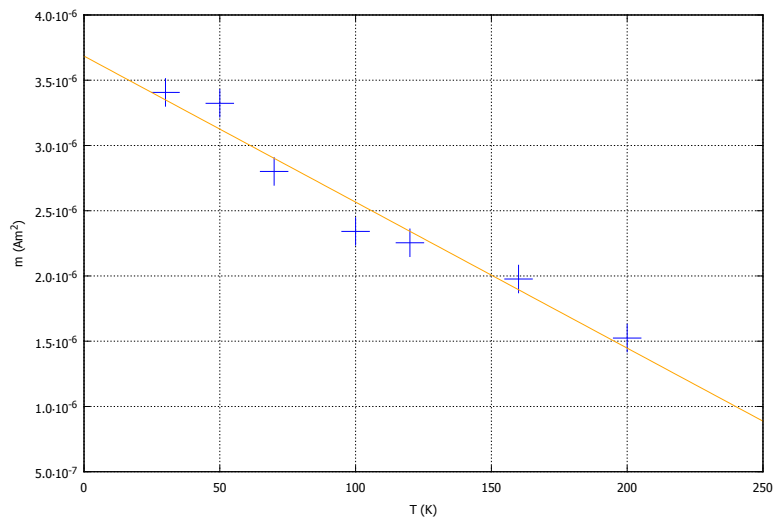
Fig. 3.6: Temperature dependence of the saturation magnetization of the ferritin sample. The values are from the fit of eq. 1.10 to the magnetization data of the ferritin sample. The solid line is a linear fit to the data points.
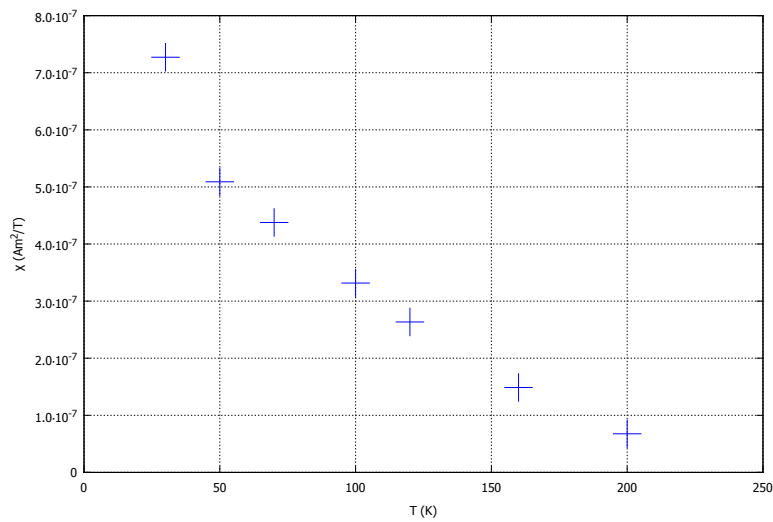
Fig. 3.7: Temperature dependence of the susceptibility of the linear term in eq. 1.10. The values are from the fit of eq. 1.10 to the magnetization data of the ferritin sample.
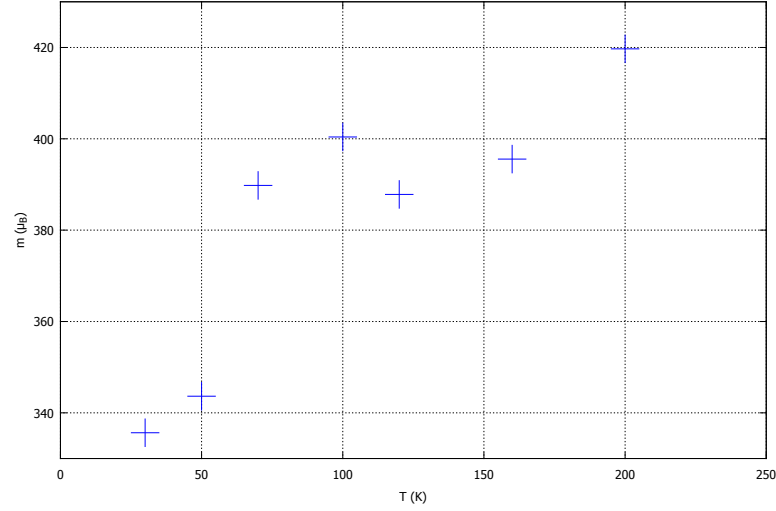
Fig. 3.8: Temperature dependence of the magnetic moment of one single ferritin nano particle in the sample. The magnetic moment is denoted in multiples of the Bohr magneton. The values are from the fit of eq. 1.10 to the magnetization data of the ferritin sample.

measured in a SQUID magnetometer. Magnetic field dependent measurements were performed at 5 K to minimize thermal noise. The measurements of the temperature dependence were performed as zero field and field cooled measurements from 5 K to 200 K. The tissue samples were freeze dried and then mounted with vacuum grease on the aluminium sample holder. Furthermore the tissue was weighted to normalize the signal to the mass of the samples which makes it possible to compare the signals of the different tissues. For statistical reasons and to minimize the possibility of contamination from the environment we measured three biological replicates of every tissue type.

3.2.1   Liver

The liver is a tissue containing a lot of blood present which also leads to a high ferritin concentration. The magnetic field dependence of the magnetic moment is shown in fig. 3.9.
A background subtraction was not necessary because the signal of the sample holder was small compared to the signal of the tissue.
The data from two of the three birds are in good agreement. A slight difference could be due to the sample holder or the different amount of vacuum grease used to fix the samples. The magnetic moment from the third bird (A409) does not really fit to the other signals. It three times larger and does not saturate in the experimental field range from -7 T to 7 T. One possible explanation could be a contamination of the sample. That could explain the higher signal but the obviously high saturation field remains unexpected.
Al three signals show a hysteresis at 5 K, because the temperature is lower than the superparamagnetic blocking temperature and the spins are blocked which result in a remanent magnetic
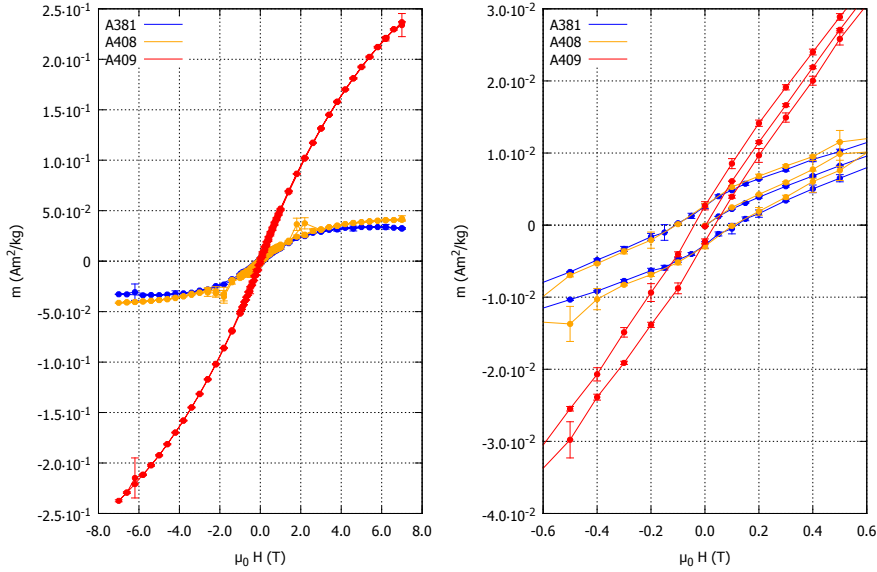
Fig. 3.9: Magnetic moment of the liver normalized to the mass as a function of the applied magnetic field at 5 K. The measurement was done with tissues from three different birds. The right graph shows a close up of the small field region. There was no background subtraction performed because the signal of the sample holder was smaller the the signals of the samples. The errorbars show the standard deviation of the averaged ten measurements.

moment. The remanent magnetic moments of all three samples have the same magnitude, just the coercive field is different for one of the samples.

The temperature dependent measurements of the magnetic moment were done as zero field and field cooled measurements with an applied magnetic field of 5 T. In fig. 3.10 the signals from all three tissues are shown. The sample from bird A409, that showed a different behaviour in the magnetic field dependence, is also different in the temperature dependent measurement. It shows a higher magnetic moment at low temperatures than the other two samples which agrees with the result shown in fig. 3.9. Another interesting behaviour happens around 50 K in all three samples. The magnetic moment forms a peak in the zero field cooled branch there. In fig. 3.11, fig. 3.12 and fig. 3.13 the signals are shown for the samples from bird A381, A408 and A409, respectively. In two of them (A381 and A408) the shape of the peak is comparable, with a peak on the zero field cooled branch and a flattening of the field cooled branch at temperatures below the peak. Moreover the magnetic moment on the field cooled branch bifurcate from the zero field cooled branch at a temperature higher than the temperature at which the peak occurs. After the bifurcation the magnetic moment of the field cooled branch is smaller than the magnetic moment of the zero field cooled branch. At temperatures below the temperature where the peak occurs the magnetic moment of the field cooled branch becomes larger than the magnetic moment of the zero field cooled branch.
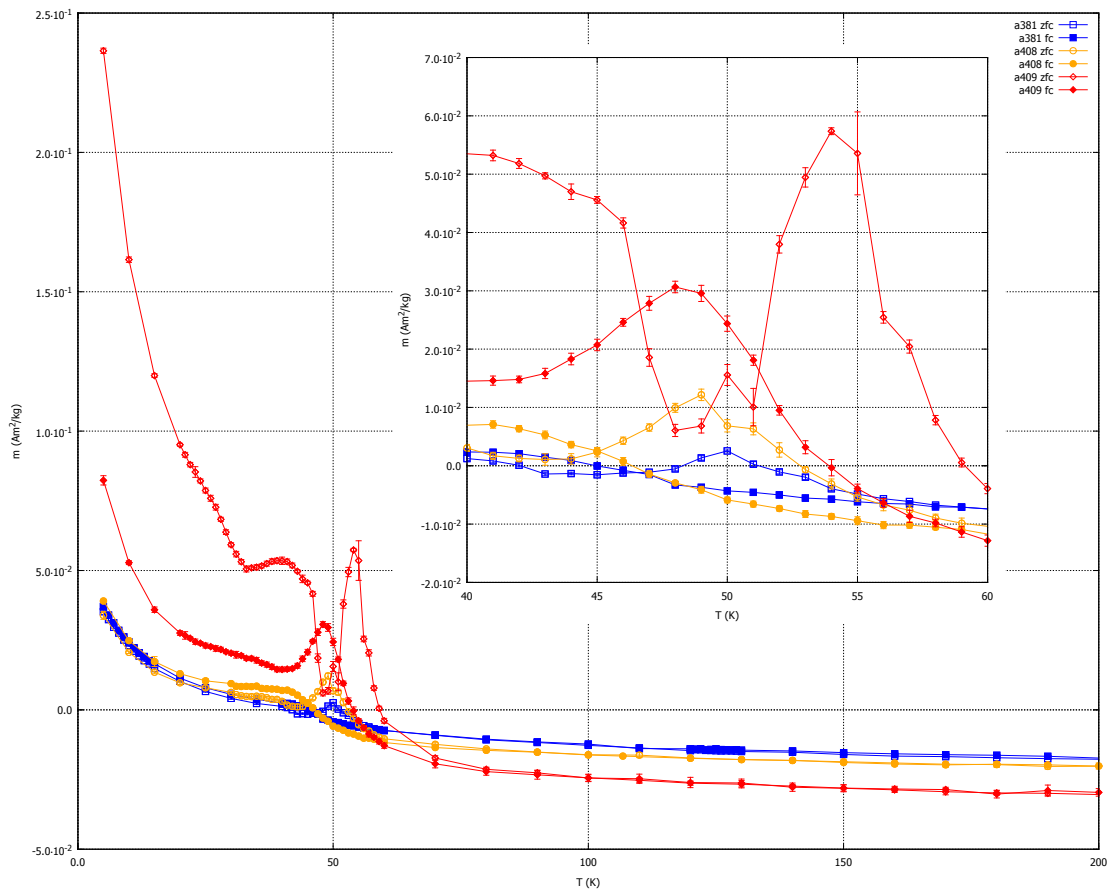
Fig. 3.10: Normalized magnetic moment of the liver at an applied field of 5 T as a function of the temperature. The zero field and field cooled curves are plotted for the three different samples. The errorbars show the standard deviation of the averaged ten measurements.

The curve of the liver from A409, shown in fig. 3.13, behaves differently. There the magnetic moment on the field cooled branch is smaller then the one on the zero field cooled branch. Surprisingly there is a peak in the field cooled signal that corresponds to a minimum in the zero field cooled branch. This is interesting because for the field cooled measurement the sample was cooled in 5 T which should align all the spins and result in a higher magnetic moment than in the zero field cooled measurement.

In all three samples the magnetic moment at 5 K is different for zero field cooling and field cooling. This corresponds to a hysteresis in the magnetic-loop measurements of all three samples. It is not clear why the remanent magnetic moment of all three samples has the same magnitude, but the difference between the magnetic moment at 5 K for zero field and field cooled measurement is different in all three samples.
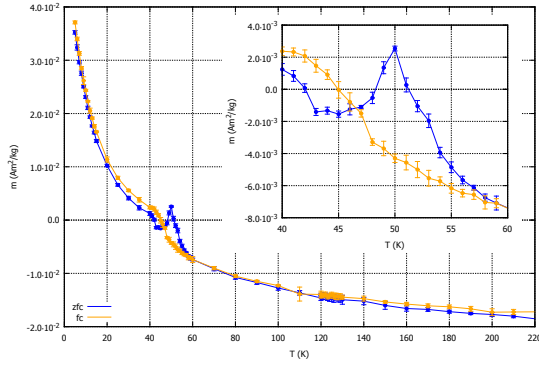
Fig. 3.11: Normalized magnetic moment of the liver from bird A381 at an applied field of 5 T as a function of the temperature. The errorbars show the standard deviation of the averaged ten measurements.
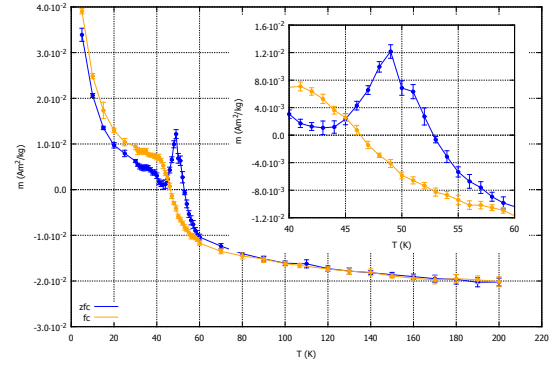
Fig. 3.12: Normalized magnetic moment of the liver from bird A408 at an applied field of 5 T as a function of the temperature. The errorbars show the standard deviation of the averaged ten measurements.
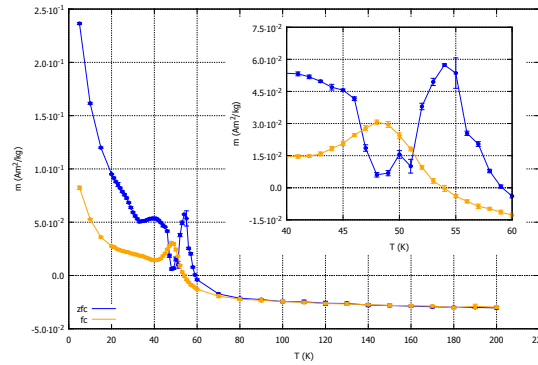

Fig. 3.13: Normalized magnetic moment of the liver from bird A409 at an applied field of 5 T as a function of the temperature. The errorbars show the standard deviation of the averaged ten measurements.
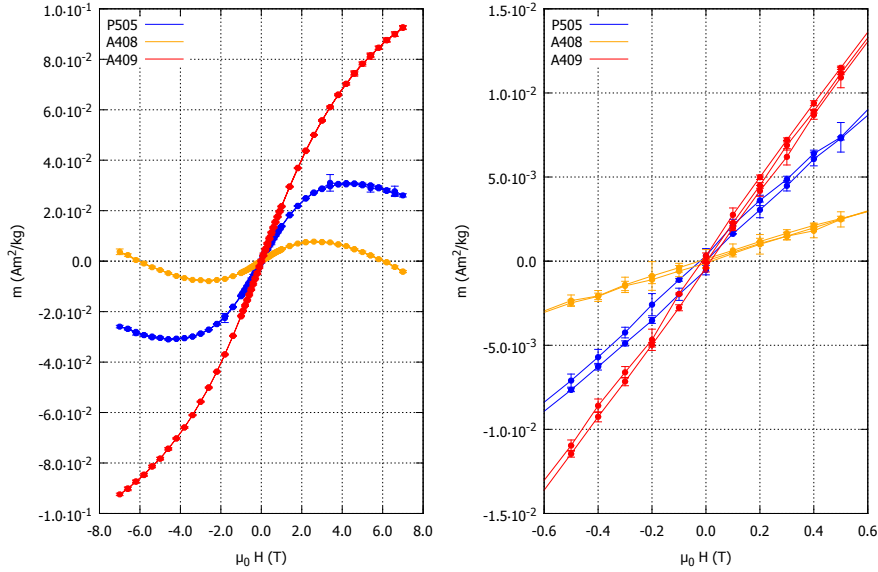
Fig. 3.14: Normalized magnetic moment of the spleen normalized as a function of the applied magnetic field at 5 K. The measurement was done with tissues from three different birds. The right graph shows a close up of the low field region. There was no background subtraction performed because the signal of the sampleholder was much smaller than the signals of the samples. The errorbars show the standard deviation of the averaged ten measurements.

3.2.2   Spleen

The spleen works primarily as a blood filter. Moreover the spleen plays an important roll in the immune system, for example most of the antibodies are synthesised there. The spleen removes old red blood cells and metabolizes their haemoglobin, so the tissue contains a lot of blood. This should, like in the liver, result in a big magnetic moment. The magnetization loops of the spleen of three different birds are shown in fig. 3.14.

Although the magnetic moments are normalized to the mass in fig. 3.14 the three different tissue samples do not behave in the same way. The signal of the samples from bird P505 and A408 show a saturate of the paramagnetic contribution in the measured interval, but with different values. This could result from a different iron concentration in the tissue. They also show a diamagnetic component that is not from the sampleholder but from the tissue itself.

The signal of the sample from bird A409 is monotonous in the measured interval, behaving in a similar way as the liver from the same bird (see fig. 3.9). No hysteresis can be observed in the close up of fig. 3.14. The hysteresis is present ether if there is ferromagnetic material in the sample or if the superparamagnetic material is below its blocking temperature. The measurement was done at 5 K which is probably higher than the blocking temperature.

A measurement of the magnetic moment as a function of the temperature was taken for all three samples. The results are shown in fig. 3.15. As in the liver, a peak occurs in the zero field cooled
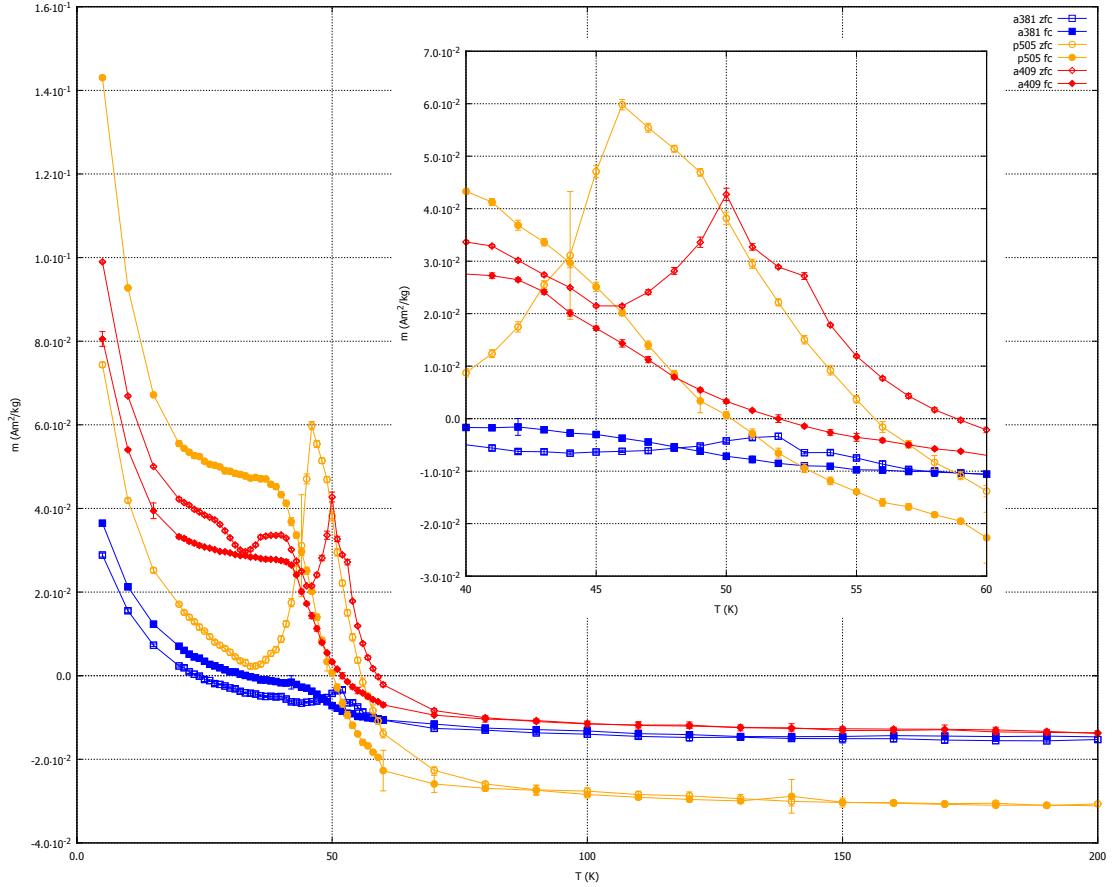
Fig. 3.15: Normalized magnetic moment of the spleen at an applied field of 5 T as a function of the temperature. The zero field and field cooled curves are plotted for the three different samples. The errorbars show the standard deviation of the averaged ten measurements.

measurement around 50 K. The results for the sample from bird A381, P505 and A409 are shown in fig. 3.16, fig. 3.17 and fig. 3.18, respectively.

The temperature dependence of the magnetic moment from the sample of bird A381 and P505 has the same shape, but the magnitudes are different. This could result from a different iron concentration in the tissue which would also describe the different saturation magnetizations shown in fig. 3.14. Apart from the magnitude, the shape of these tow tissue samples is similar to the temperature dependence of the magnetic moment in two of the three liver samples. The tissue from bird A409 shows a different behaviour which is also the case for the tissue from the liver of this bird.

In contrast to the measurements of the liver samples, the samples from the spleen do not show a hysteresis at 5 K. However, there is a difference in the magnetic moment at 5 K for the zero field and field cooled measurement. Normally that should correspond to a hysteresis in the magnetic-loop measurements.
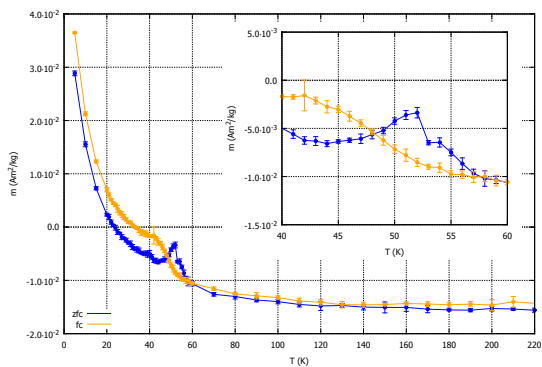
Fig. 3.16: Normalized magnetic moment of the spleen from bird A381 at an applied field of 5 T as a function of the temperature. The errorbars show the standard deviation of the averaged ten measurements.
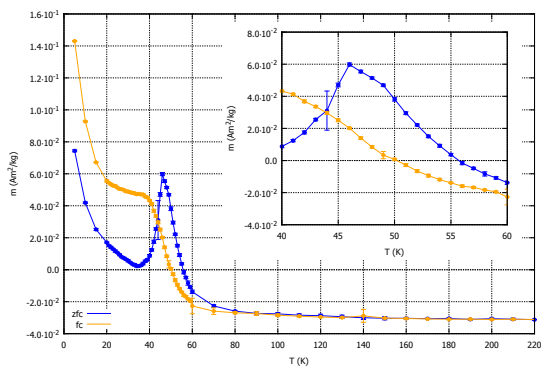
Fig. 3.17: Normalized magnetic moment of the spleen from bird P505 at an applied field of 5 T as a function of the temperature. The errorbars show the standard deviation of the averaged ten measurements.
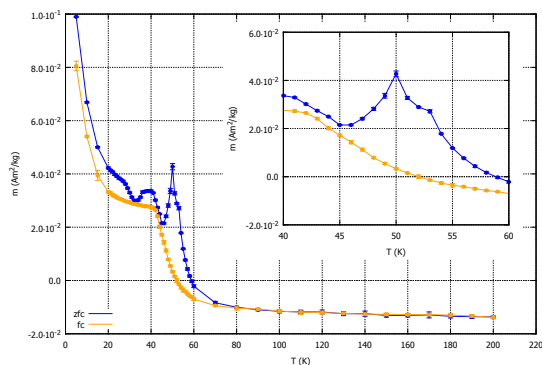
Fig. 3.18: Normalized magnetic moment of the spleen from bird A409 at an applied field of 5 T as a function of the temperature. The errorbars show the standard deviation of the averaged ten measurements.
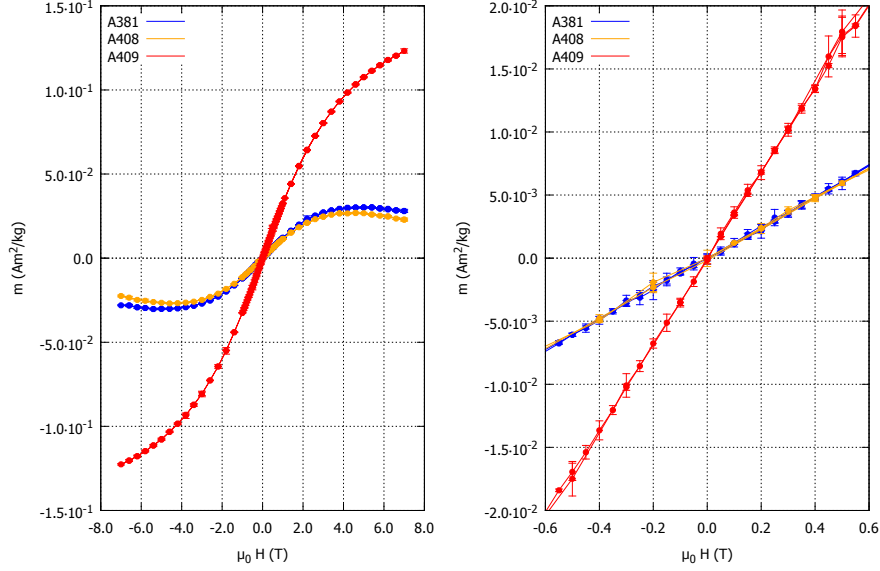
Fig. 3.19: Normalized magnetic moment of the heart as a function of the applied magnetic field at 5 K. The measurement was done with tissues from three different birds. The right graph shows a close up of the low field region. There was no background subtraction performed because the signal of the sample holder was much smaller than the signals of the samples. The errorbars show the standard deviation of the averaged ten measurements.

3.2.3   Heart

The heart is a muscular organ responsible for circulating blood in an organism. The magnetic moment of a reference tissue as a function of the applied field at 5 K is shown in fig. 3.19.

The tissues from bird A408 and A381 behave similarly, but the tissue from bird A409 behaves differently as in the measurements of the liver and the spleen. There is again no saturation of the paramagnetic contribution in the measurement interval and a higher signal compared to the samples of the other birds. Because that happened in the liver, spleen and heart of the same bird it could be due to the blood concentration in the tissue. Contamination from exogenous sources in all three tissues is not very likely. Moreover the samples from the birds A408 and A409 were dissected with the same procedure and right after each other, so any contamination from the lab environment should be distributed more or less randomly over this two birds.

No hysteresis can be seen in the right graph of fig 3.19, so the blocking temperature if any lies below 5 K where the measurement was performed.

The magnetic moment as a function of the temperature is shown in fig. 3.20. Comparing the three curves the one of the sample from bird A409 shows a bigger magnetic moment than the other two. This is in agreement with the higher signal of this sample in the magnetic-loop measurements. The temperature dependence of the single samples is shown in fig. 3.21, fig. 3.22 and fig. 3.23 for the samples of bird A381, A408 and A409, respectively.
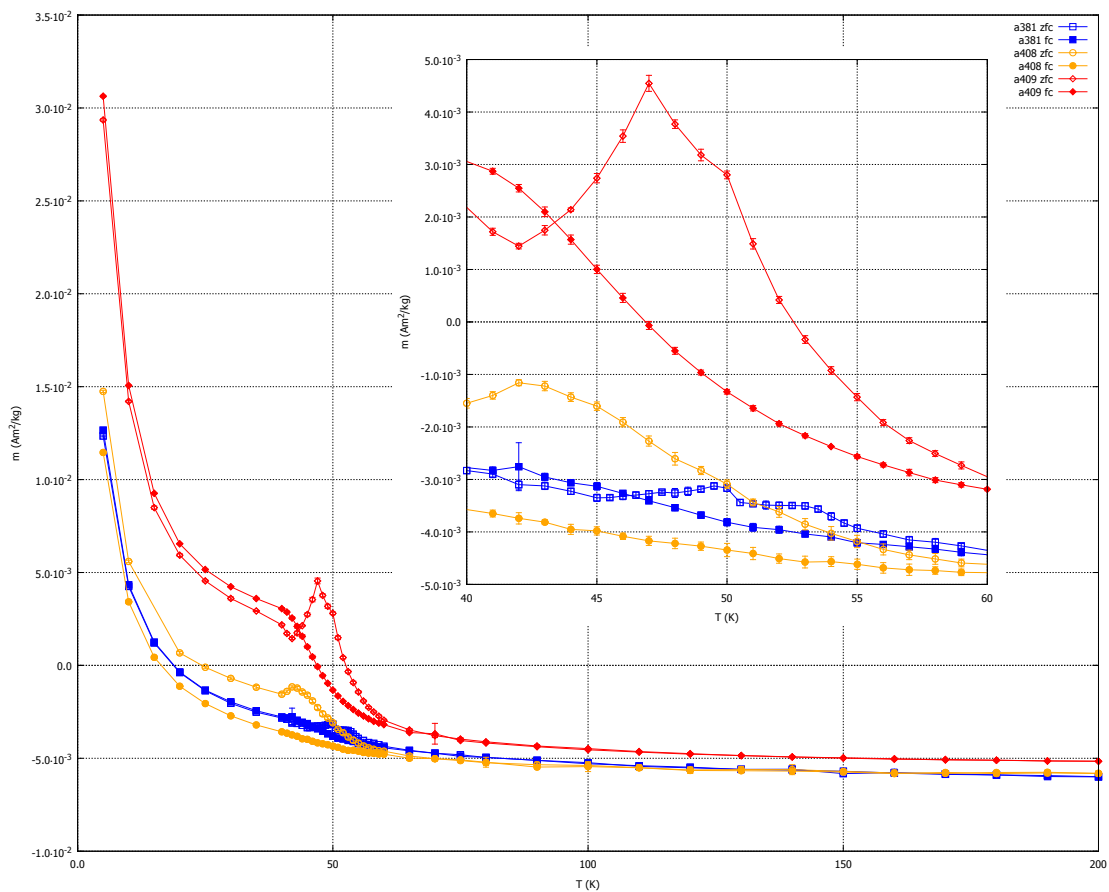
Fig. 3.20: Normalized magnetic moment of the heart at an applied field of 1 T as a function of the temperature. The zero field and field cooled curves are plotted for the three different samples. The errorbars show the standard deviation of the averaged ten measurements.

A peak at 50 K is found in the samples of A381 and A409. The shape of the peak is similar to the shape of the peaks in the liver and the spleen samples. In sample A408 it is shifted to lower temperatures and has a slightly different shape. In all heart tissue samples the peak is not as high as in the spleen or the liver samples. At 5 K a difference between the magnetic moment measured after zero field or field cooling is found, however, like the spleen no hysteresis occurs in the magnetic-loop measurements.
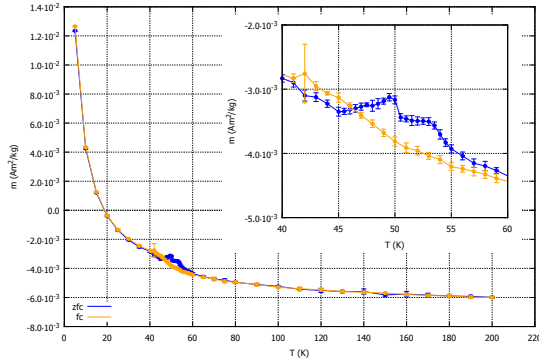
Fig. 3.21: Normalized magnetic moment of the heart from bird A381 at an applied field of 1 T as a function of the temperature. The errorbars show the standard deviation of the averaged ten measurements.
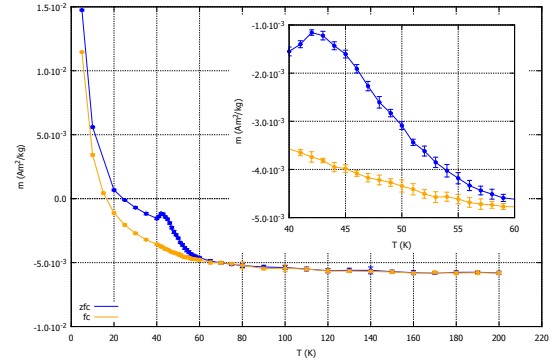
Fig. 3.22: Normalized magnetic moment of the heart from bird A408 at an applied field of 1 T as a function of the temperature. The errorbars show the standard deviation of the averaged ten measurements.
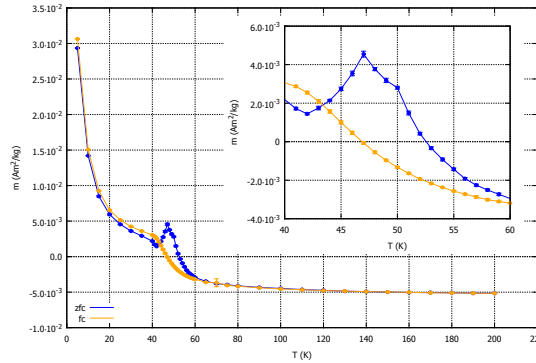
Fig. 3.23: Normalized magnetic moment of the heart from bird A409 at an applied field of 1 T as a function of the temperature. The errorbars show the standard deviation of the averaged ten measurements.
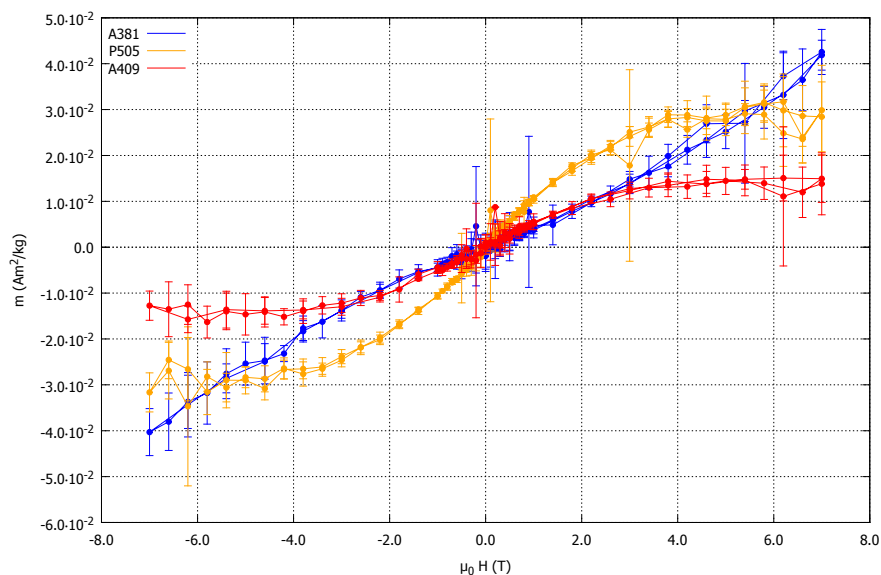
Fig. 3.24: Normalized magnetic moment of the olfactory bulbs as a function of the applied magnetic field at 5 K. The signal from the sample holder was subtracted from the measured data. The measurement was done with tissues from three different birds. The errorbars show the standard deviation of the averaged ten measurements.

3.2.4   Olfactory bulbs

The olfactory bulbs are a structure in the brain responsible for processing input from the primary olfactory receptors. The magnetic moment of the sample tissue as a function of the applied field at 5 K is shown in fig. 3.24. The plotted data are corrected by the signal of the sample holder.

The measured signals were all in the order of several 10^{-8}Am^2 with a standard deviation of several 10^{-9}Am^2. A saturation is visible in the curves of the tissues from bird P505 and A409. The curves show the expected shape but saturate at different values, which could be due to different iron concentration in the different tissues. The curve of the tissue from bird A381 shows an unexpected behaviour because there is no saturation of the paramagnetic contribution in the whole measurement range. Therefore it is important to compare the measured signal with the signal from the sample holder, which is shown in fig. 3.25. One can see that the signal of the sample on the sample holder is just slightly bigger than the signal of the sample holder alone. The subtraction of these two signals with similar magnitude leads to a bigger noise of the resulting signals. Therefore the resulting signal is hard to interpret. The signal of the tissue of bird A381 is so small because the tissue sample is smaller than the ones of the other two birds.

A measurement of the temperature dependence of the magnetic moment was not done because the signals were small at 5 K and would decrease further with increasing temperature. It is not possible to measure the magnetic moment in small structures of such a small signal.
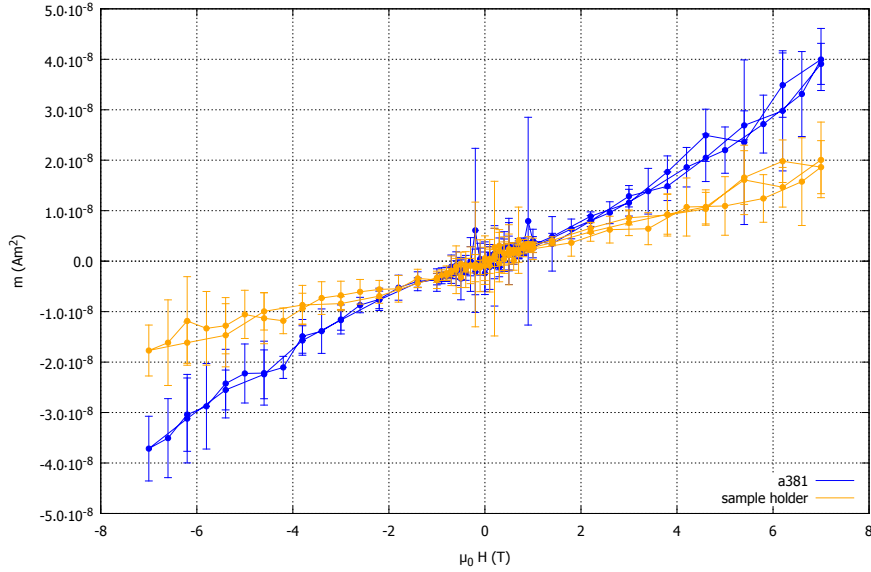
Fig. 3.25: Magnetic moment of the olfactory bulbs of bird A381 and the sample holder as a function of the applied magnetic field. The errorbars show the standard deviation of the averaged ten measurements.

3.2.5   Hippocampus

The hippocampus is a region in the brain which is responsible for memory and spatial navigation [20]. It could be involved in the processing of a signal from a magnetoreceptor, or the magnetoreceptor itself might reside within the hippocampus. The magnetic moment of sample tissue as a function of the applied field is shown in fig. 3.26.

The behaviour of the three samples under an applied magnetic field is very different. The tissue from bird A409 has a diamagnetic background and an overlaid paramagnetic signal. In the measurement range the paramagnetic signal saturates. The tissue of bird P505 has no diamagnetic background and the paramagnetic contribution of the signal does not saturate in the measurement interval. In the high field range a linear increase as in ferritin is observed. The tissue from bird A381 shows a very noisy linear increase. This signal has to be interpreted with caution because the mass of the sample is small compared to the others. The signal of the hippocampus tissue of bird A381 and the signal of the sample holder alone is shown in fig. 3.27. One can see that the signal of the sample and the one of the sampleholder are more or less the same. Therefore the signal of the hippocampus of bird A381 is below the detection limit of the SQUID magnetometer.

No temperature dependence of the magnetic moment was measured because the signals where in general extremely small at 5 K.
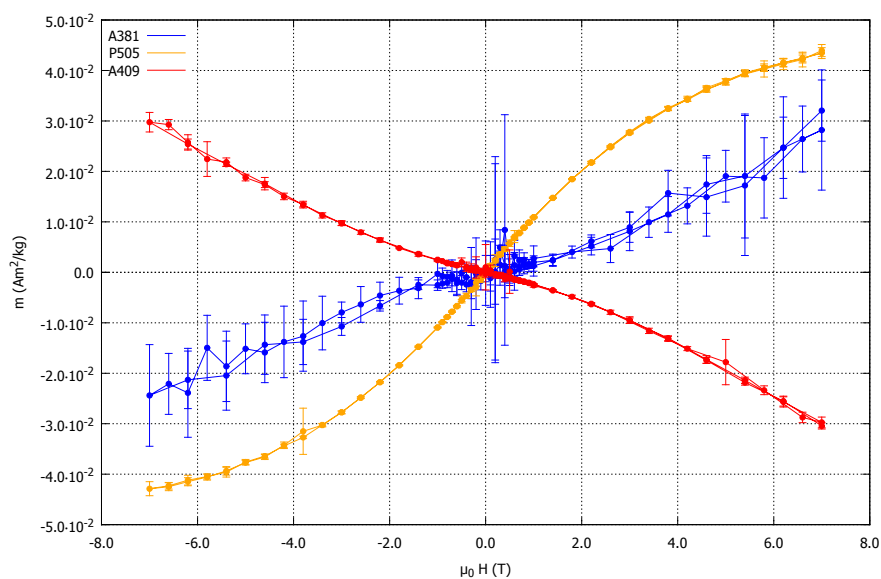
Fig. 3.26: Normalized magnetic moment of the hippocampus as a function of the applied magnetic field at 5 K. The shown data is without any background or sample holder subtraction. The measurement was done with tissue from three different birds. The errorbars show the standard deviation of the averaged ten measurements.
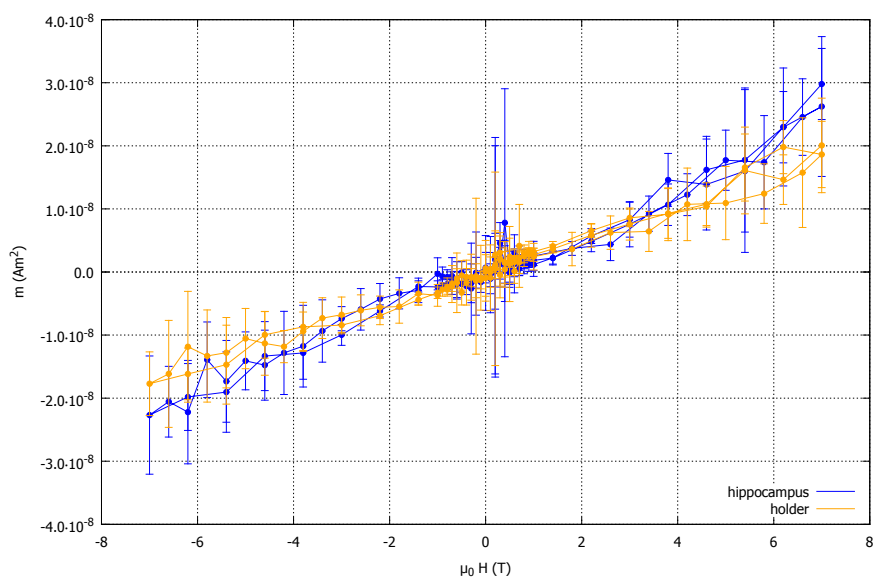
Fig. 3.27: Magnetic moment of the hippocampus of bird A381 and the sampleholder as a function of the applied magnetic field. The errorbars show the standard deviation of the averaged ten measurements.
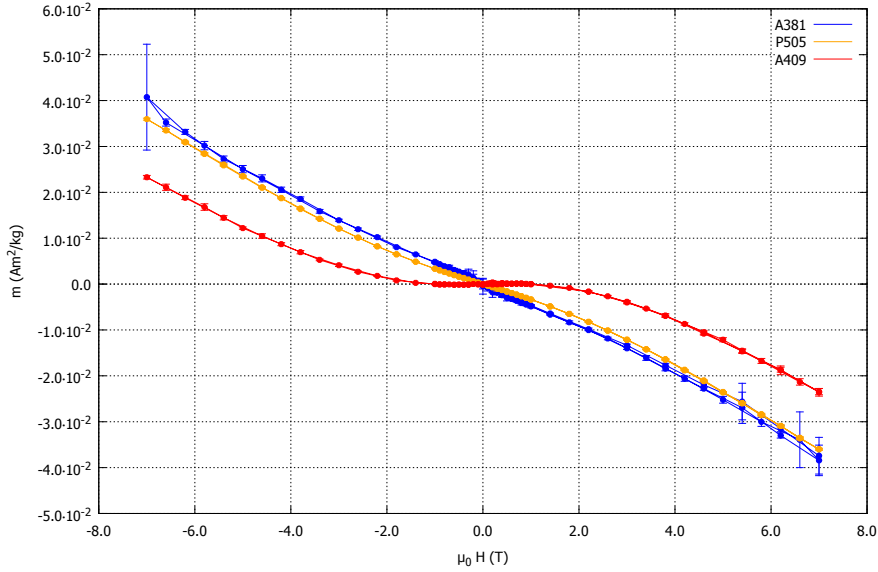
Fig. 3.28: Normalized magnetic moment of samples of the respiratory concha as a function of the applied magnetic field at 5 K. There was no background or sample holder subtraction done. The measurement was done with tissues from three different birds. The errorbars show the standard deviation of the averaged ten measurements.

3.2.6   Respiratory concha

The respiratory concha is part of the avian respiratory system in the beak. It has been shown that iron-rich cells are located in this region, leading to the speculation that they may have magnetic properties. The magnetic moments of tissue samples from three birds as a function of applied magnetic field are shown in fig. 3.28.

The curves of the tissue from bird A381 and P505 show the same behaviour. The small difference could be due to a different amount of vacuum grease for the fixation. All three signals are a superposition of a diamagnetic signal and a paramagnetic signal that saturates in the measurement interval. The diamagnetic contribution, which is almost the same in all three samples, is most significant at higher fields. The paramagnetic contribution of the tissue from bird A409 is stronger than that of the other two tissue samples. This could be explained by a higher iron concentration in the tissue from bird A409.

A hysteresis was not observed in any of the signals, so there is no remanent magnetization at 5 K.

3.2.7   Upper beak

The measurement was done with the skin of the upper beak. This tissue was used because the upper beak was discussed as a location for a putative magnetoreceptor [16]. The magnetic
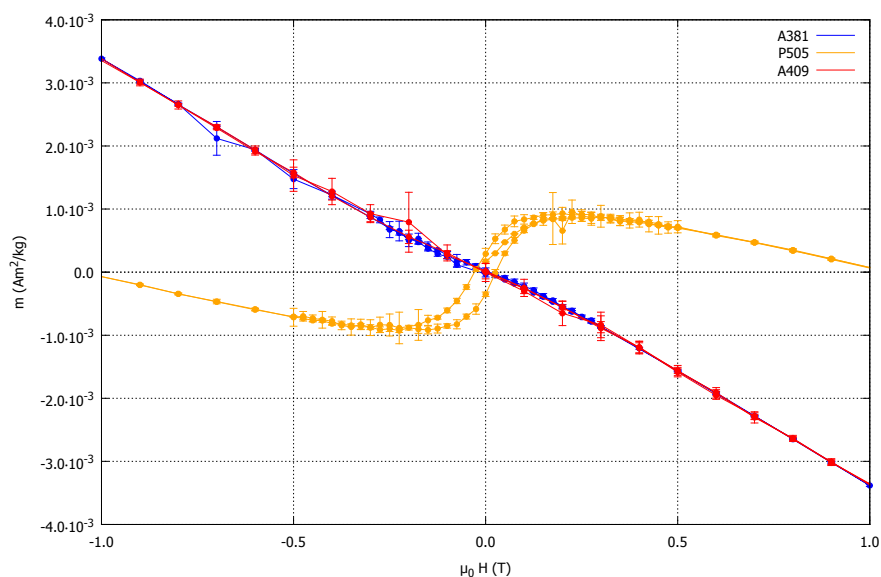
Fig. 3.29: Normalized magnetic moment of the upper beak as a function of the applied magnetic field at 5 K. The measurement was done with tissues from three different birds. The errorbars show the standard deviation of the averaged ten measurements.

moment as a function of the applied field is shown in fig. 3.29.

In the magnetization curves of the samples from bird A381 and A409 only a diamagnetic signal occurs. A possibly superimposed paramagnetic signal was below the detection range of the SQUID magnetometer. The magnetization curve of the sample form bird P505 shows hysteresis which was present up to the body temperature of the pigeon. Nevertheless, because the hysteresis was found only in one of the three samples it is most likely caused by contamination. That could happen easily because the upper beak is directly exposed to the environment and the contamination might originate for instance from the cage of the pigeon.

3.2.8   Iron content

The iron content of different tissue samples was obtained from TXRF spectroscopy (see sec. 2.2). This method was chosen because it allows to detect trace elements in the sample. The iron concentration of different tissues is shown in fig. 3.30.

The iron concentrations of the two upper beaks explain the magnetic behaviour shown in fig. 3.29. There the tissue from bird P505 showed a hysteresis and the one from bird A381 did not. Comparing the iron concentration one finds that the value of the upper beak from bird P505 is more then double the corresponding value of bird A381. Furthermore, a large concentration of copper was found in the upper beak from bird P505. These results support the theory that the hysteresis in fig. 3.29 comes from contamination and not from the sample itself.

The biggest iron concentration was found in the spleen because it contains most blood of the
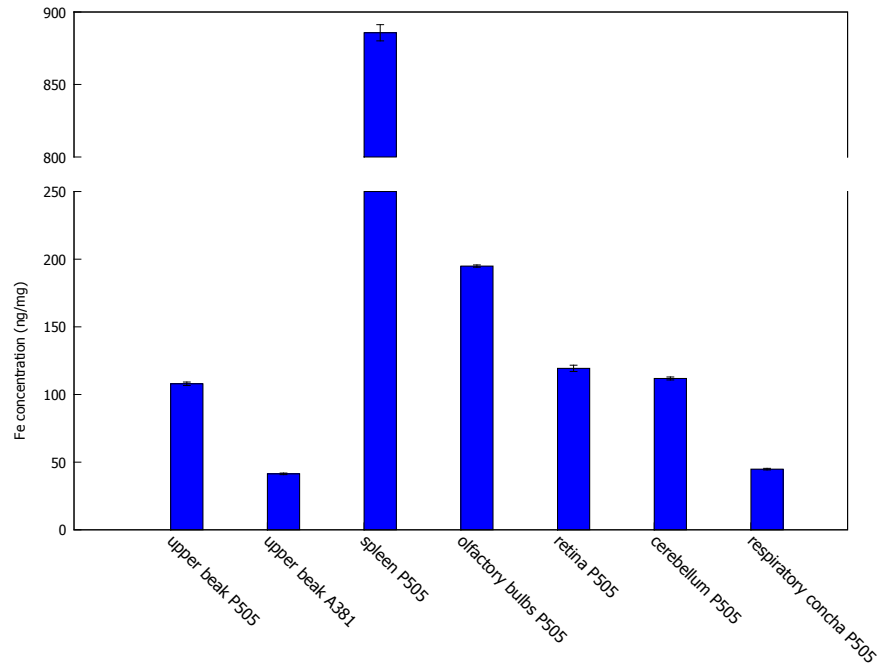
Fig. 3.30: Iron content in the different tissues. The error bars represent the fit error of the fit from the ideal spectrum to the measured signal.

measured samples. In the brain regions, cerebellum and olfactory bulbs, more iron was detected than in the samples from the beak.

3.3 The cuticulosome as a magnetoreceptor

The cuticulosome is an iron rich structure in the hair cells in the inner ear of the homing pigeon (see sec. 1.4) [6]. Further characterisations in the Keays Lab showed that the iron in the cuticulosome is mainly stored in ferritin. The hair cells with the cuticulosomes are in the cochlea. We measured that structure but the signal was to weak to be detected with the SQUID magnetometer because of the small available mass. However, with our measurements of ferritin and the TEM images of the cochlea from [6] one can now estimate the magnetic properties of the cuticulosome.

The magnetic moment of one ferritin protein is approximately $m_{ferritin} \approx 350 \mu_{Bohr}$. The number of ferritins in one cuticulosome can be estimated from its size. The diameter of the cuticulosome is approximately 500 nm and the diameter of the iron rich core of ferritin is approximately 8 nm. This results in $N = 4.5 \, 10^5$ ferritin nano particles in one cuticulosome.

The single ferritin particles in the cuticulosome are too far apart to order magnetically, because at room temperature the thermal energy is higher than any interaction energy between the magnetic moments. Therefore the cuticulosome is a paramagnet with the magnetic moments of the ferritins randomly distributed. If there is a magnetic field applied to the cuticulosome the thermally fluctuating magnetic moments align in a certain fraction with the applied field. This makes it possible to describe the magnetic properties of the cuticulosome with the Langevin function $L(x) = \coth x - \frac{1}{x}$. The magnetic moment of the cuticulosome reads as follows:

$$m_{cuticulosome} = N m_{ferritin} L \left(\frac{m_{ferritin} B}{k_B T} \right) \tag{3.1}$$

One can now calculate the magnetic moment of one cuticulosome in the earth's magnetic field at the body temperature of a pigeon.

$$m_{cuticulosome}(B_{earth} = 50 \, \mu T, T = 310 \, \text{K}) = 1.6 \, 10^{-20} \, \text{Am}^2 \tag{3.2}$$

The detection limit for our SQUID magnetometer is around $10^{-11} \, \text{Am}^2$. So one would need at least 10^9 cuticulosomes or around 10^3 cochleas to be able to measure a magnetic moment of the cochlea. However, by knowing the magnitude of the magnetic moment it is still possible to calculate interactions with the earth's magnetic field. TXRF measurements of the cochlea yield the total iron content of the tissue. Therefore the contribution of the cuticulosome can not be separated from the contribution of the surrounding tissue to the total iron content. That makes it not possible to measure only the iron stored in the cuticulosome with TXRF spectroscopy.

The earth's magnetic field has a small gradient for the scale of a pigeon. Therefore it is not possible that a detectable force acts directly on the cuticulosome, however, a torque might be induced which activates a force sensitive channel in a cell membrane. For this to be possible the magnetic moment of the cuticulosome has to point not in the same direction as the earth's magnetic field. This is possible for a highly anisotropic cuticulosome, because the magnetic
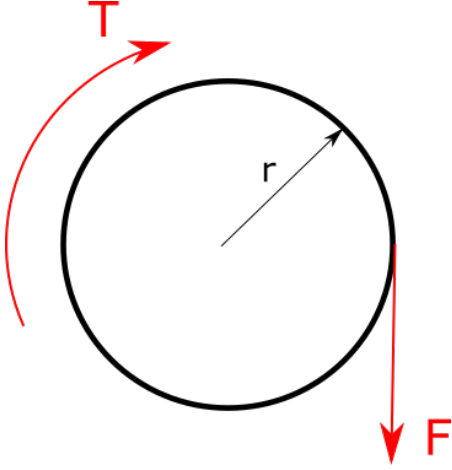
Fig. 3.31: Torque on the cuticulosome and the resulting force on the surface.
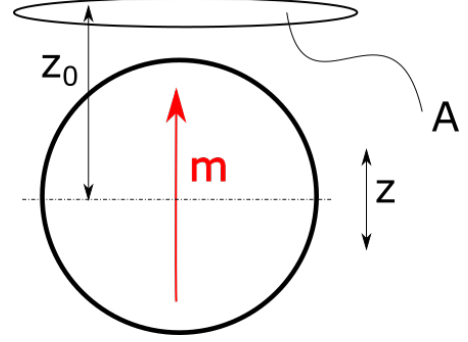
Fig. 3.32: The cuticulosome with magnetic moment m oscillating along z. In the surface A at the distance z_0 there is a voltage induced that could be detected by the biological system.

moment arises from a magnetization in the earth's magnetic field and for a spherical cuticulosome it would point in the same direction.

For the biggest effect let's assume that the cuticulosome is magnetized perpendicular to the earth's magnetic field. That is not very likely but gives a estimation for the maximal possible force. The torque of a magnetic moment in an external magnetic field is defined as follows

$$\vec{T} = \vec{m} \times \vec{B} \tag{3.3}$$

Assuming that $\vec{m}$ and $\vec{B}$ are perpendicular the force at the surface of the cuticulosome is the following:

$$F = \frac{m\,B}{r} = \frac{1.6 \cdot 10^{-20} \cdot 50 \cdot 10^{-6}}{250 \cdot 10^{-9}}\,\text{N} = 3.2 \cdot 10^{-18}\,\text{N} \tag{3.4}$$

This is illustrated in fig. 3.31.

It is reported that channels can detect several 10^{-12} N [17]. With the unlikely assumption that the magnetic moment and the earth's magnetic field are perpendicular to each other the resulting force is still six orders of magnitude away from a detectable signal. It seams unlikely that the cuticulosome acts as a torque magnetoreceptor.

Cuticulosomes are located in hair cells which are used to detect sound. They oscillate with the frequency of the sound that the animal hears ($\sim$ Hz to $\sim$ 6 kHz [21]). The cuticulosome is magnetized in the earth's magnetic field and oscillates with the hair cell. One could now imagine a surface not moving or moving in antiphase to the cuticulosome. At this surface there could be a voltage induced that is further detected. As shown in fig. 3.32 the surface is assumed to be perpendicular to the magnetic moment. This is the orientation where the biggest voltage is induced in the surface because the magnetic field of the dipole moment changes most in its z-direction.

The induced voltage in a loop with the enclosed surface A is the following:

$$u = - \int \frac{\partial \vec{B}}{\partial t} d\vec{A} \tag{3.5}$$

The magnetic field of a magnetic moment is a dipole field:

$$\vec{B}_{dipole} = \frac{\mu_0}{4\pi} \left(\frac{3 \left(\vec{m} \cdot \vec{r} \right) \vec{r}}{r^5} - \frac{\vec{m}}{r^3} \right) \tag{3.6}$$

One can now calculate the induced voltage in a loop with the enclosed surface shown in 3.32. The parameters are chosen in a way that they fit in the cellular environment. The distance of the surface to the centre of the cuticulosome is $z_0 = 4\,\mu$m. It oscillates for $z = 2\,\mu$m at a frequency of $f = 10\,$kHz. Because the induced voltage is bigger for higher frequencies the highest detectable frequency for a pigeon is taken. The radius of the loop with the enclosed surface A where the induction is taking place is $r = 3\,\mu$m.

The voltage calculated with this parameters is of the order of 10^{-16} V. This is orders of magnitude smaller than the detectable voltages of 10^{-6} V in an electroreceptor of a ray [18]. This big difference of the detectable and estimated induced voltage makes it very unlikely that such a mechanism is used to detect the earth's magnetic field.

4 Conclusion

In this thesis the magnetic properties of a variety of tissues from the pigeon were measured. This was done for the first time, which makes it very difficult to interpret the results because there are no comparable measurements. The results show that the magnetic moment of single samples do not fit the others. This could have several reasons, like the amount of blood in the tissue. Comparing the signal from blood in sec. 2.4 with other tissues shows that the majority of the signal from the tissue samples originates from the blood in them. These influences are hard to remove and therefore it is very important to measure tissue from at least three different animals to make sure that the signals are from the tissue alone. Moreover the measurement of the upper beak showed how easy it is to get contamination in a sample. The measured hysteresis in one sample would encourage the theory of a magnetoreceptor in the upper beak, but it resulted from contamination as the other two tissue samples and the iron content measurement with TXRF showed.

The magnetic behaviour can be arranged in two groups. One is the group of the tissues containing much blood like the spleen, the liver and the heart. There the superparamagnetic behaviour of the ferritin is visible in the measurements. This is also the reason for the hysteresis that is present in the samples with a blocking temperature above 5 K. In contrast to that, the samples show a saturation of the paramagnetic contribution in the measurement interval, not like ferritin where a linear increase is superimposed. It is not clear why no such increase is observed in the tissue samples.

The second group is made of the samples from the beak, like the respiratory concha or the upper beak skin. They show a diamagnetic behaviour superimposed with a smaller paramagnetic signal. This could be because of the low blood content in the beak and the remaining tissue behaves like a diamagnet. The paramagnetic contribution could arise from some blood or other iron in the beak. No hysteresis occurs in the measurements of the magnetic moments as a function of the applied field, except for the contaminated upper beak. So the tissues do not have a remanent magnetization big enough that it could be measured in the SQUID magnetometer.

The characterisation of the samples from the brain is difficult because their signal was very small. They tend to behave like paramagnets, but there is not enough data to clarify that.

In the measurements of the spleen, the liver and the heart we found a peak in the magnetic moment after zero field cooling at 50 K. The peaks have not all the same shape, but most of them look similar. However, all of them have in common that they appear around 50 K, which is surprising because it happened in three biological replicas of three different tissue types. What all of the samples have in common is that they contain a lot of blood and therefore a lot of ferritin. However, the measurement of the temperature dependence of the magnetic moment of ferritin did not show such a peak, which is also shown in [3]. The measurements in [3] and in this thesis were performed with horse spleen ferritin. In [23] the temperature dependence of human liver ferritin was measured and they have also not found a peak at 50 K. Furthermore the behaviour could come from the blood. One blood sample was measured to estimate the contribution to

the signals from tissues and no peak at 50 K was found in the temperature dependence of the magnetic moment. For a better description of this effect measurement techniques that access the spin structure of the sample are necessary. One explanation could be that the anitferromagnetic and ferromagnetic ordering of the spins lead to a spin frustration. Then it depends on the cooling process if the spins order anitferromagnetic or ferromagnetic. Spin frustration is an effect that happens in spin glasses.

Another aim of the thesis was to access the magnetic properties of the cuticulosome. It consists of ferritin nano particles which makes it important to understand the magnetic properties of ferritin for the description of the cuticulosome. An estimation of the magnetic moment of the cochlea, where the cuticulosomes are placed, showed that the magnetic moment is too small to measure it in a SQUID magnetometer. However, with the knowledge of the magnetic properties of ferritin it was possible to quantify the interaction between the cuticulosome and the earth's magnetic field. This calculations showed that the resulting torque or induced voltage from the interaction with the earth magnetic field are very small. They are even smaller then the thermal noise in the cells. This shows that it is hardly possible to imaging the cuticulosome as a magnetoreceptor working with one of these two mechanisms without further modifications. It would be necessary that the signal from the earth's magnetic field is amplified to a range where the biological system can detect it. Such a process is difficult to realize if the cuticulosome as a magnetoreceptor were based on a torque detection mechanism. For the induction based mechanism one would need a big magnetic field that changes with time at the position of the induction loop. This could be the case on the surface of the cuticulosome where the dipole approximation is not true any more and one has to take the single ferritins into account. There the magnetic dipole fields of the single ferritins are stronger than the earth's magnetic field. However, the magnetic moments are still small and the loop has to be fixed or move in antiphase with respect to the cuticulosome. Moreover the detection process of the induced voltage in such a loop is also not totally clear.

There are still open questions, but electromagnetic induction remains a good candidate for the mechanism behind magnetorecepton. The movement of the head of the pigeon could generate the changing magnetic field and conducting liquids in the inner ear could function as the loop where a voltage is induced. However, such a magnetoreceptor would require a very sensitive electroreceptor to be able to detect a magnetic field as small as the earth's magnetic field.

5 Outlook

The description of the peak in the temperature dependence measurements of the magnetic moments from several tissues in three different animals is still open. It seams that there are several mechanism superimposed, which makes it very difficult to describe the phenomena. Measurements that access the spin structure of the sample, like small angle neutron scattering, Mössbauer spectroscopy or muon spin spectroscopy, are necessary for a better understand.

List of Figures

References

[1] Néel, L. (1952). Théorie du traînage magnétique de diffusion. Journal de Physique et le Radium, 13(5), 249-264.

[2] Bean, C. P., Livingston, J. D. (1959). Superparamagnetism. Journal of Applied Physics, 30(4), S120-S129.

[3] Makhlouf, S. A., Parker, F. T., Berkowitz, A. E. (1997). Magnetic hysteresis anomalies in ferritin. Physical Review B, 55(22), R14717.

[4] Mike McElfresh, Fundamentals of magnetism and magnetic measurements featuring quantum design's magnetic property measurement system, Quantum Design, 1994.

[5] Klockenkaemper, Reinhold, and Alex von Bohle, Total-reflection X-ray Fluorescence Analysis and Related Methods, John Wiley & Sons, 2014.

[6] Lauwers, M., Pichler, P., Edelman, N. B., Resch, G. P., Ushakova, L., Salzer, M. C., ... Keays, D. A. (2013). An iron-rich organelle in the cuticular plate of avian hair cells. Current Biology, 23(10), 924-929.

[7] Mouritsen, H. (2015). Magnetoreception in birds and its use for long-distance migration. Sturkie's Avian Physiology, 113-133.

[8] Wiltschko, W., Wiltschko, R. (1995). Migratory orientation of European robins is affected by the wavelength of light as well as by a magnetic pulse. Journal of Comparative Physiology A, 177(3), 363-369.

[9] Hore, P. J., Mouritsen, H. (2016). The Radical-Pair Mechanism of Magnetoreception. Annual review of biophysics, (0).

[10] Solov'yov, I. A., Greiner, W. (2007). Theoretical analysis of an iron mineral-based magnetoreceptor model in birds. Biophysical journal, 93(5), 1493-1509.

[11] Jungerman, R. L., Rosenblum, B. (1980). Magnetic induction for the sensing of magnetic fields by animals—an analysis. Journal of theoretical biology, 87(1), 25-32.

[12] Faivre, D., Schuler, D. (2008). Magnetotactic bacteria and magnetosomes. Chemical Reviews, 108(11), 4875-4898.

[13] Binns, C. (2010). Introduction to nanoscience and nanotechnology (Vol. 14). John Wiley & Sons.

[14] Chasteen, N. D., Harrison, P. M. (1999). Mineralization in ferritin: an efficient means of iron storage. Journal of structural biology, 126(3), 182-194.

[15] Wu, L. Q., Dickman, J. D. (2012). Neural correlates of a magnetic sense. science, 336(6084), 1054-1057.

[16] Hanzlik, M., Heunemann, C., Holtkamp-Rötzler, E., Winklhofer, M., Petersen, N., & Fleissner, G. (2000). Superparamagnetic magnetite in the upper beak tissue of homing pigeons. Biometals, 13(4), 325-331.

[17] Howard, J., Hudspeth, A. J. (1988). Compliance of the hair bundle associated with gating of mechanoelectrical transduction channels in the bullfrog's saccular hair cell. Neuron, 1(3), 189-199.

[18] Kalmijn, A. J. (1977). The electric and magnetic sense of sharks, skates, and rays. Oceanus, 20(3), 45-52.

[19] Chen, L., Bazylinski, D. A., Lower, B. H. (2010). Bacteria that synthesize nano-sized compasses to navigate using earth's geomagnetic field. Nature Education Knowledge, 1(10), 14.

[20] Bingman, V. P., Hough, I. I., Kahn, M. C., Siegel, J. J. (2003). The homing pigeon hippocampus and space: in search of adaptive specialization. Brain, Behavior and Evolution, 62(2), 117-127.

[21] Heffner, H. E., Heffner, R. S. (2007). Hearing ranges of laboratory animals. Journal of the American Association for Laboratory Animal Science, 46(1), 20-22.

[22] Handbook of chemistry and physics. 57th edition. 1976-1977

[23] Dubiel, S. M., Zablotna-Rypien, B., Mackey, J. B., Williams, J. M. (1999). Magnetic properties of human liver and brain ferritin. European biophysics journal, 28(3), 263-267.